

# Correlated activity of periodically driven binary networks

Tobias Kühn<sup>1</sup> and Moritz Helias<sup>1,2</sup>

<sup>1</sup>*Institute of Neuroscience and Medicine (INM-6) and Institute for Advanced Simulation (IAS-6) and JARA BRAIN Institute I, Jülich Research Centre, Jülich, Germany*

<sup>2</sup>*Department of Physics, Faculty 1, RWTH Aachen University, Aachen, Germany*

(Dated: November 30, 2018)

Experiments showed that excess synchronous spike events are locked to the phase of beta-oscillations in the local field potential (LFP) more strongly than spikes that appear in isolation [Denker et al. 2011, Cereb. Cortex]. To identify the mechanisms by which correlations depend on the phase of the LFP, which primarily reflects input activity, we examine a balanced network of homogeneously connected binary model neurons receiving input from a sinusoidal perturbation. Its temporal evolution is described by Glauber dynamics, which is simulated and investigated analytically. Applying mean-field theory and treating the periodic input in linear response theory, the cyclostationary mean activities and pairwise zero-time-lag correlations are analytically computed. They agree with their simulated counterparts over a wide parameter range. We find that correlations are time dependent by two distinct mechanisms, one due to the modulated susceptibility (via the external input and network feedback) and one due to the time-varying autocorrelations. For some parameters, this leads to resonant correlations even if mean activities show non-resonant behavior. Our results can help to answer the salient question how oscillations in mesoscopic signals and spike correlations interact.

## AUTHOR SUMMARY

In network theory, statistics are often considered to be stationary. While this assumption can be justified by experimental insights to some extent, it is often also made for reasons of simplicity. However, the time-dependence of statistical measures do matter in many cases. For example, time-dependent processes are examined for gene regulatory networks or networks of traders at stock markets. Periodically changing activity of remote brain areas is visible in the local field potential (LFP) and its influence on the spiking activity is currently debated in neuroscience. In experimental studies, however, it is often difficult to determine time-dependent statistics due to a lack of sufficient data representing the system at a certain time point. Theoretical studies, in contrast, allow the assessment of the time dependent statistics with arbitrary precision. We here extend the analysis of the correlation structure of a homogeneously connected EI-network consisting of binary model neurons to the case including a global sinusoidal input to the network. We show that the time-dependence of the pairwise correlations - to first order - can be explained analytically. We expose the mechanisms that modulate correlations in time and show their dependence on the effectively inhibitory recurrent network feedback and on neurons acting as low-pass-filters on their input. These generic properties carry over to more realistic neuron models.

## INTRODUCTION

As the local field potential (LFP) is a quantity that can be measured relatively easily, this mesoscopic signal is experimentally well documented. Its interpretation is, however, still debated. For example, changes in the amplitude of one of the components of the spectrum of the LFP have been attributed to changes in behavior (cf. e.g. [1]).

The local field potential is a valuable window into the dynamics of neuronal networks that is complementary to the spiking activity of individual neurons or small groups thereof: It is composed of the superposition of the activity of hundreds of thousands to millions of neurons [2, 3] and forward modeling studies have confirmed [4] that it is primarily driven by the synaptic inputs to the local network [5–7]. This is also the hypothesis behind the interpretation given by Denker et al. [8] for the observation that the simultaneous activation of neurons above chance level is strongly locked to a certain phase of the oscillatory component of the LFP in the beta-range. The authors provide a conceptual model in which an increase in the local input - visible in the LFP - leads to the activation of so called cell assemblies, groups of neurons that are connected more strongly among each other than to other neurons.

To investigate the mechanisms found experimentally in an analytically tractable case, we here present the simplest model that we could come up with and that captures the most important features: A local network receiving periodically changing external input. The randomly connected neurons receive sinusoidally modulated input, interpreted as originating from other brain areas, which mimics the major source of the experimentally observed LFP. Extending the analysis of mean activities and correlations in the stationary state [9–11], we aim to expose the fundamental mechanisms that shape the correlations in these periodically driven networks. This goal guides our choice of the level of detail of our model. It is “minimal” in the sense that we will lose important properties if we further simplify it. Earlier works [10, 12, 13] showed that our setup without sinusoidal drive is sufficient to qualitatively reproduce and explain phenomena observed in vivo, like high variability of neuronal activity and small correlations. The latter point can be explained in binary networks by the suppression of fluctuations by inhibitory feedback, which is a general mechanism also applicable to other neuron models [14] and even finds application outside neuroscience, for example in electrical engineering [15]. The high variability observed in binary networks can be explained by the network being in the balanced state, that robustly emerges in the presence of negative feedback [12, 16]. In this state, the mean excitatory and inhibitory synaptic inputs cancel so far that the summed input to a neuron fluctuates around its threshold. This explanation holds also for other types of model networks and even for biological neural networks [17]. The first crucial feature of the models considered here is hence their operation in the balanced state.

Secondly, a network of homogeneously connected binary neurons implements the general feature of neuronal networks that every neuron receives input from a macroscopic number of other neurons, letting the impact of a single synaptic afferent on the activation of a cell be small and the summed input be distributed close to Gaussian: For uncorrelated incoming activity, the ratio between the fluctuations caused by a single input and the fluctuations of the total input is  $N^{-\frac{1}{2}}$ , independent of how synapses scale with  $N$ . However, the input to a neuron is actually not independent, but weakly correlated, i.e. the correlations decay at least as fast as  $\frac{1}{N}$  [12, 13]. Therefore this additional contribution to the fluctuations also decays like  $N^{-\frac{1}{2}}$ . Third, a threshold-like nonlinearity determines the activation of a neuron. This feature is shared by the binary, the leaky integrate-and-fire and, approximately, also the Hodgkin-Huxley model neuron. Fourth, an important property shared by all neuron models is that the activity of one cell

effects the downstream neurons on average for the duration of a characteristic time  $\tau$ . For binary neurons, this time scale is identical to the mean interval  $\tau$  between updates, because, once active, a neuron will stay active until the next update. At that point it most certainly deactivates, because we here consider low activity states prevalent in cortex [18]. In the leaky integrate-and-fire model the exponentially decaying membrane voltage with time constant  $\tau$  has a similar effect. As a consequence, neurons transmit their input in a low-pass filtered manner to their output (see [19, 20] for the leaky integrate-and-fire model, [21] for the exponential integrate-and-fire model, and [22] for the quadratic integrate-and-fire model).

Intuitively, one might expect that a global drive only influences the mean activity, but not higher order moments. Instead, we will here show how each of the four above-mentioned fundamental properties of neuronal networks shape and give rise to the mechanisms that cause time-dependent correlations. As these properties are generic, the exposed mechanisms are robust and are therefore expected to appear also in models of higher biological realism and complexity. Moreover, the fluctuations in recurrent networks of binary neurons show a structure similar to that in spiking networks [23]. In contrast to spiking models, however, the correlated fluctuations in binary networks can be readily understood with elementary mathematical tools from Markov systems, linear algebra, and systematic perturbation theory.

We derive analytical expressions for the first order corrections to the mean activities and correlations. They show reasonable agreement with the results of the simulation of the binary network performed with NEST [24, 25] and the numerical implementation of the coupled system of non-linear ordinary differential equations of the moment hierarchy truncated at second order.

## RESULTS

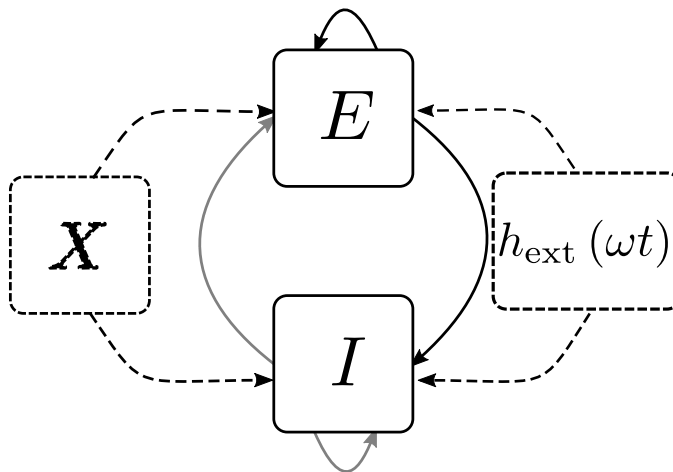


Figure 1. **Recurrent balanced network driven by oscillatory input.** Recurrently connected excitatory ( $E$ ) and inhibitory ( $I$ ) populations (Erdős-Rényi random network with connection probability  $p$ ) receiving input from an external ( $X$ ) excitatory population. Additionally, all neurons in the microcircuit receive an additional sinusoidal signal of amplitude  $h_{\text{ext}}$  and frequency  $\omega$ , representing the oscillatory activity received from external brain areas.

Our “minimal” model consists of one inhibitory ( $I$ ) population and, in the later part of the paper, additionally one excitatory population ( $E$ ) of binary neurons [9, 12, 26], which are recurrently and homogeneously connected and driven by a global sinusoidal input mimicking the incoming oscillatory activity that is visible in the LFP, illustrated in Figure 1. In the second and third case, the local network additionally gets input from an external excitatory population ( $X$ ), representing the surrounding of the local network and increasing the variability in the local network. Uncorrelated noise in the input has the same effect on the marginal statistics of each neuron, but the fluctuations imprinted by the external population, due to shared inputs, in addition drive the pairwise correlations within the network [11, c.f. especially the discussion]. Therefore we need the external population  $X$  to arrive at a realistic setting including all sources of pairwise correlations.

In the following, we will extend the analysis of cumulants in networks of binary neurons in [9–11, 27]. This formal analysis allows us to obtain analytical approximations for the experimentally observable quantities, such as pairwise correlations. In contrast to these prior works, we consider not stationary, but time-dependent correlations.

To give an example, we illustrate in Figure 2 the meaning of a time-dependence of the correlation between two signals  $x_1(t)$  and  $x_2(t)$  in a simpler setting, before embarking on the analysis of the correlated dynamics emerging in the recurrent network setting (Figure 1). The covariance is defined as  $c(t) = \langle \delta x_1(t) \delta x_2(t) \rangle = \langle (x_1(t) - \langle x_1(t) \rangle) (x_2(t) - \langle x_2(t) \rangle) \rangle$ , where  $\langle \dots \rangle$  denotes the average over realizations. In the example, the two signals are composed of a superposition of a deterministic sinusoidal component and fluctuations from three sources: One of the random processes contributes to both signals and the other two processes are each specific to one of them (formal details can be found in section ). In the beginning of the time frame under consideration, both signals are fed by nearly the same noise. At later times, the common part decreases until nearly zero, as indicated by the decay of the correlation coefficient shown in the middle part of Figure 2E. In the region with correlation coefficients close to one (i.e. nearly exclusively “common noise”), it is clearly visible in Figure 2C that the fluctuations of  $a$  closely follow those of  $b$ , whereas for correlations close to zero, the fluctuations are nearly independent. Plotting several realizations of process 1 on the  $x$ - and of process 2 on the  $y$ -axis (scatter plot) leads to a lengthy ellipse for the first case (Figure 2B) and circle-like ellipses in the second (Figure 2D). Figure 2A and C show that the time-dependence of pairwise correlations is hard to detect “by eye” because the “raw signal” in panel A shows quite clearly the time-dependence of the first cumulant (the mean value), but the time-dependence of the second cumulant (the pairwise correlation) is only visible after subtracting the mean (Figure 2C). Given a stochastic model that allows the calculation of arbitrary empirical estimates, it is easy to disentangle the time dependence of the different cumulants, whereas in experimental studies it is impossible to measure the instantaneous mean activity exactly. This leads to problems determining the correct time-dependence of pairwise correlations and related quantities in the experiment, necessitating a theoretical study to understand the prevalent mechanisms. In the following we will identify these mechanisms by which time-dependent correlations of activities arise in oscillatory-driven recurrent networks.

### Binary network model and its mean field equations

Here, we consider binary model neurons that at each point in time are either inactive  $n_i = 0$  or active  $n_i = 1$ . The time evolution of the network follows the Glauber dynamics [28], so the neurons are updated asynchronously. At every infinitesimal time step  $dt$ , any neuron is chosen with probability  $\frac{dt}{\tau}$ . After an update, neuron  $i$  is in the state 1 with the probability  $F_i(\mathbf{n})$  and in the 0-state with probability  $1 - F_i(\mathbf{n})$ , where the activation function  $F$  is chosen to be

$$F_i(\mathbf{n}) = H(h_i - \theta_i)$$

$$h_i = \sum_{k=1}^N J_{ik} n_k + h_{\text{ext}} \sin(\omega t) + \xi_i$$

$$H(x) = \begin{cases} 1 & \text{if } x \geq 0 \\ 0 & \text{if } x < 0 \end{cases}.$$
(1)

We introduced the connectivity matrix  $J$  with the synaptic weights  $J_{ij} \in \mathbb{R}$  describing the influence of neuron  $j$  on neuron  $i$  and being negative for an inhibitory, positive for an excitatory neuron  $j$ . By  $J$ , the outcome of the update of neuron  $i$  potentially depends on the state  $\mathbf{n} = (n_1, \dots, n_N)$  of all other neurons in the network. Compared to the equations in [11, page 4], we here added an external sinusoidal input to the neurons representing the influence of other cortical or subcortical areas and Gaussian uncorrelated noise with  $\langle \xi_i \rangle = 0$  and  $\langle \xi_i \xi_j \rangle = \delta_{ij} \sigma_{\text{noise}}^2$ . The threshold  $\theta_i$  depends on the neuron type and will be chosen according to a desired mean activity.

For simulations, we employ the neural simulation package NEST [24, 25]. Analytical results are obtained by mean-field theory [9–11, 13, 29, 30] and are described for reasons of completeness and consistency of notation in section . We here only note the main steps and assumptions entering the approximations. The basic idea is to describe the time evolution of the Markov system in terms of its probability distribution  $p(\mathbf{n})$ . Using the master equation (13), we obtain ordinary differential equations (ODEs) for the moments of  $p(\mathbf{n}, t)$ . The dynamics couples moments of arbitrarily high order. To close this set of equations, we neglect cumulants of order higher than two, which amounts to approximating also the input by a stochastic variable with cumulants vanishing for orders higher than two, i.e. by a Gaussian [31]. This can be justified by noticing that the number of neurons contributing to the input is high and their activity is weakly correlated, which makes it plausible that the central limit theorem is applicable. For the

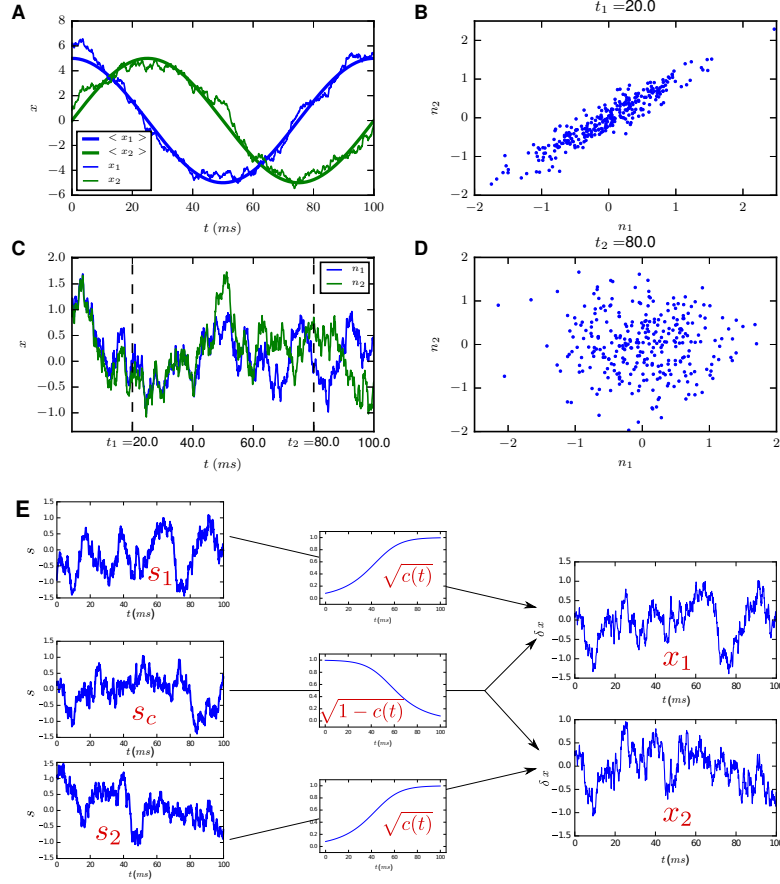


Figure 2. **Example of two signals with time-dependent correlation.** **A** Two noisy signals ( $m_1(t)$ ,  $m_2(t)$ , thin curves) and their expectation values ( $\langle x_i(t) \rangle$ ),  $i \in \{1, 2\}$  (thick curves). **C** Differences  $n_i := \delta x_i(t) = x_i(t) - \langle x_i(t) \rangle$  between the signals  $i = 1, 2$  and their respective averages, i.e. the noise component of the signal. **B** Scatter plot of  $\delta x_2(t_a)$  versus  $\delta x_1(t_a)$  for multiple realizations for a fixed time point  $t_a = 20$  (indicated by dashed vertical line in **C**) with high correlation. **D** Same as **B**, but for a time point  $t_b$  with low correlation (dashed vertical line in **C**). **E** Schematics of the creation of the correlated noise  $(n_1, n_2)^T$ . Technical details of the implementation of the processes are given in section .

population averaged mean activities  $m_\alpha$ , variances  $a_\alpha$ , and cross correlations  $c_{\alpha\beta}$

$$m_\alpha(t) := \frac{1}{N_\alpha} \sum_{i \in \alpha} \langle n_i(t) \rangle \quad (2)$$

$$a_\alpha(t) := \frac{1}{N_\alpha} \sum_{i \in \alpha} \left( \langle n_i(t) \rangle - \langle n_i(t) \rangle^2 \right) \quad (3)$$

$$c_{\alpha\beta}(t) := \frac{1}{N_\alpha N_\beta} \sum_{i \in \alpha, j \in \beta, i \neq j} \langle n_i(t) n_j(t) \rangle - \langle n_i(t) \rangle \langle n_j(t) \rangle, \quad (4)$$

we get with  $K_{\alpha\beta} = p_{\alpha\beta} N_\beta$  (and  $p_{\alpha\beta}$  the probability that there is a synapse from a neuron in population  $\beta$  to a neuron in population  $\alpha$  and  $N_\alpha$  the size of the population, i.e. the connection probability) being the number of synapses from  $\beta$  to  $\alpha$  the ODEs

$$\tau \frac{d}{dt} m_\alpha(t) = -m_\alpha(t) + \varphi(\mu_\alpha(\mathbf{m}(t), h_{\text{ext}} \sin(\omega t)), \sigma_\alpha(\mathbf{m}(t), c(t))) \quad (5)$$

$$\tau \frac{d}{dt} c_{\alpha\beta}(t) = \left\{ -c_{\alpha\beta}(t) + \sum_\gamma \left[ S(\mu_\alpha(\mathbf{m}(t), h_{\text{ext}} \sin(\omega t)), \sigma_\alpha(\mathbf{m}(t), c(t))) \cdot K_{\alpha\gamma} J_{\alpha\gamma} \left( c_{\gamma\beta}(t) + \delta_{\gamma\beta} \frac{a_\beta(t)}{N_\beta} \right) \right] \right\} + \{\alpha \leftrightarrow \beta\}, \quad (6)$$

where  $\alpha \leftrightarrow \beta$  stands for the transposed term. Here  $\varphi$  is the expectation value of the activation function, which is smooth (though the activation function itself is a step function, therefore not even continuous), fulfills  $\lim_{\mathbf{m} \rightarrow 0} \varphi = 0$  and  $\lim_{\mathbf{m} \rightarrow 1} \varphi = 1$ , monotonously increases and its derivative  $S$  with respect to  $\mu$  has a single maximum and is largest for the mean input  $\mu$  within a region with size  $\sigma$  around the threshold  $\theta$ .  $S$  measures the strength of the response to a slow input and is therefore termed susceptibility. The exact definitions are given in the methods part in (17), (18), (19) and (20).

The stationary solution of the ODEs (5) and (6) can be found by solving the equations

$$\overline{\mathbf{m}} = \varphi(\overline{\mathbf{m}}) \quad (7)$$

$$2\overline{c} = SKJ \left( \overline{c} + \frac{\overline{a}}{N} \right) + \text{transposed} \quad (8)$$

numerically and self-consistently, as it was done in [9, 11, 13]. We indicate stationary solutions of the ODEs by a bar. Whether we solve (7) first neglecting the influence of the pairwise correlations and solve then (8) or solve both equations simultaneously, taking into account the effect of correlations on  $\sigma_\alpha$  in (19), only causes a marginal difference. For the analytical determination of the first Fourier coefficients of mean activities and correlations, we anyway neglect the time-dependence of  $\sigma$ . Therefore neglecting the dependence of  $\overline{\sigma}$  on  $\overline{c}$  is consistent with the calculations for the time-dependent case (cf. the considerations between (21) and (22)). The full time-dependent solution of (5) and (6) can, of course, be determined numerically without any further assumptions. Besides the comparison with simulation results, this will give us a second check for the linear perturbation theory. To calculate results analytically, which will allow us to identify the major mechanisms, we will linearize the equations around the stationary solutions, in the following denoted by a bar. We only keep the linear term of order  $h_{\text{ext}}$  of the deviation, justifying a Fourier ansatz for the solutions. For the mean activities, this results in  $m_\alpha(t) = \overline{m}_\alpha + \delta m_\alpha(t) = \overline{m}_\alpha + M_\alpha^1 e^{i\omega t}$  with

$$M_\alpha^1 = U_{\alpha\beta} M_1^\beta = U_{\alpha\beta} \frac{h_{\text{ext}} (U^{-1} S(\overline{\mu}, \overline{\sigma}))^\beta (-i\tau\omega + 1 - \lambda_\beta)}{(\tau\omega)^2 + (1 - \lambda_\beta)^2}. \quad (9)$$

Here  $U$  is the matrix representing the basis change that transforms  $\overline{W}_{\alpha\beta} := S(\overline{\mu}_\alpha, \overline{\sigma}_\alpha) K_{\alpha\beta} J_{\alpha\beta}$  into a diagonal matrix with  $\lambda_\alpha$  the corresponding eigenvalues. We see that, independent of the number of populations or the detailed form of the connectivity matrix, the amplitude of the time-dependent part of the mean activities has to first order in  $h_{\text{ext}}$  the shape of a low-pass-filtered signal and therefore the phases of  $\delta \mathbf{m}$  will lag behind the external drive and its amplitude decreases asymptotically like  $\frac{1}{\omega}$  (Figure 5B), as can be seen in Figure 3, in Figure 4, and in Figure 5.

If we also separate the correlations into their stationary part and a small deviation ( $c_{\alpha\beta}(t) = \overline{c}_{\alpha\beta} + \delta c_{\alpha\beta}(t)$ , where  $\delta c_{\alpha\beta}(t) = \mathcal{O}(h_{\text{ext}})$ ), expand  $S(\mu_\alpha(t), \sigma_\alpha(t))$  and  $a(t)$  around their stationary values and keep only the terms of order  $h_{\text{ext}}$ , we get the ODE

$$\begin{aligned} & \tau \frac{d}{dt} \delta c(t) + 2\delta c(t) - \overline{W} \delta c(t) - (\overline{W} \delta c(t))^T \\ &= \left\{ \underbrace{\left[ \text{diag}(K \otimes J \delta \mathbf{m}(t)) \right]}_{\text{recurrent drive.}} + \underbrace{h_{\text{ext}} \sin(\omega t)}_{\text{direct drive.}} \right] \text{diag}\left(\frac{\partial S}{\partial \mu(t)}\right) K \otimes J \overline{c}^{\text{total}} \\ &+ \underbrace{\overline{W} \text{diag}\left(\frac{1 - 2\overline{\mathbf{m}}}{N}\right) \text{diag}(\delta \mathbf{m}(t))}_{\text{modulated-autocorrelations-drive}} \left\{ \right. \\ &+ \left. \{ \dots \}^T, \right. \end{aligned} \quad (10)$$

where we used the point-wise product  $\otimes$  (cf. (16)) and defined  $\overline{c}^{\text{total}} := (\overline{c} + \text{diag}(\frac{\overline{a}}{N}))$ . The second line contains the “susceptibility terms”, which, in turn, result from the direct effect of the external input (“direct drive”) and the effect of time-dependent recurrent feedback (“recurrent drive”).

In summary, we can now answer the question posed in the beginning: Why does a global periodic drive influence the pairwise correlations in the network at all and does not just make the mean activities oscillate? First, the autocorrelations are modulated with time, simply because they are determined via (3) by the modulated mean activities. A neuron  $i$  with modulated autocorrelation  $a_i(t)$  projects via  $J_{ji}$  and  $J_{ki}$  to two other neurons  $j, k$  and therefore shapes the pairwise correlations  $c_{ji}(t)$  and  $c_{ki}(t)$  in a time-dependent way as well. We call this effect the “modulated-autocorrelations-drive”, indicated by the curly brace in the second last line of (10). The other contributions



are a bit more subtle and less obvious, as they are absent in networks with linear activation function. The derivative of the expectation value of the activation function, the susceptibility, contributes linearly to the ODE of the pairwise correlations. As the activation function in our example is nonlinear, the susceptibility depends on the average input. This, in turn, is perturbed by the direct drive and the recurrent feedback as a response to the first, indicated by the curly braces in the second line of (10). Together, we call these two term the “susceptibility terms”.

Let us now look at the behavior of these contributions and their relation to each other. With respect to their dependence on the number of synaptic connections  $|K|$ , the sum of the two susceptibility terms is of the same order of magnitude as the modulated-autocorrelations-drive (cf. (30) f. in the section ), therefore their interplay determines the shape of the solution of (10), as can be seen e.g. in Figure 3, Figure 4, Figure 6, Figure 9 and Figure 10. The recurrent drive  $\propto K \otimes J \delta \mathbf{m}(t)$  partly cancels the direct drive  $\propto h_{\text{ext}} \sin(\omega t)$ , as the feedback  $\propto K \otimes J < 0$  in the network is effectively negative and the response  $\delta \mathbf{m}(t)$  is nearly in phase with the perturbation for low frequencies. Furthermore, the modulated-autocorrelations-drive vanishes for  $\overline{m}_\alpha = \frac{1}{2}$ . However, for realistic activity,  $\overline{m}_\alpha \ll \frac{1}{2}$ , so that the modulated-autocorrelations-drive is proportional to and thus always in anti-phase with  $\delta m_\alpha(t)$ .

We solve (10) by transforming it into the eigensystem of  $\overline{W}$  and inserting a Fourier ansatz,  $\delta c_{\alpha\beta}(t) = C_{\alpha\beta}^1 e^{i\omega t}$ . The solution consists of a low-pass filtered part coming from the direct drive and two parts that are low-pass filtered twice coming from the recurrent drive and the modulated-autocorrelations-drive. For a detailed derivation, see .

We have calculated higher Fourier modes for the simulated and the numerically generated data to check if they are small enough to be neglected, i.e. if the response is still in the regime in which the system is effectively linear. Of course, it would be possible to derive analytical expressions for those as well. However, we will see that the linear order (and, correspondingly, the first harmonic) qualitatively and for remarkably large perturbations even quantitatively gives the right predictions. We will therefore limit our analysis to controlling the behavior of higher harmonics through the numerical solution.

In the following we will study three different models of balanced neuronal networks to expose the different mechanisms in their respective simplest setting.

### Single population

Generally, the deviation of the mean activity from the stationary solution  $\delta m$  is in phase with the perturbation for  $\omega \approx 0$  and lags behind it for larger  $\omega$  due to the “forgetfulness” of the network (represented by the leak term in the ODE) and the inhibitory feedback. In the case of a single population, which has to be inhibitory in order to get a stable stationary point, average pairwise correlations are negative [cf. 11, Fig. 5]. Therefore, the two terms in the prefactor of the  $S$ -terms,  $\overline{c} + \frac{1}{N}\overline{a}$ , partly cancel, letting the  $a$ -term dominate the shape of the  $\omega$ -dependence of the correlation (Figure 3). The terms driving the time variation of the correlation are

$$\begin{aligned} & \left( \underbrace{KJ \delta m(t)}_{\substack{S_m\text{-term} \propto \frac{1}{\omega} \text{ for big } \omega}} + \underbrace{h_{\text{ext}} \sin(\omega t)}_{\substack{S_h\text{-term does not scale with } \omega}} \right) \frac{\partial S}{\partial \mu} \underbrace{\left( \overline{c} + \frac{\overline{a}}{N} \right)}_{\substack{\text{partly cancel}}} \\ & + \underbrace{\overline{W} (1 - 2\overline{m}) \frac{\delta m(t)}{N}}_{\substack{a\text{-term} \propto \frac{1}{\omega} \text{ for big } \omega}}. \end{aligned} \quad (11)$$

The susceptibility terms and the modulated-autocorrelations-drive are low-pass-filtered, leading to two  $S$ -terms and one  $a$ -term (indicated by curly braces in (11)). Because the  $S_h$ -term decays slower with growing  $\omega$  (asymptotically like  $\frac{1}{\omega}$ , because it is low-pass-filtered only once) than the  $S_m$ -term (that decays asymptotically like  $\frac{1}{\omega^2}$ , because it is low-pass-filtered twice, like the  $a$ -term) and they have opposite signs, the absolute value of their sum has a maximum at a certain frequency (shown in Figure 3C, purple curve). This maximum is overshadowed by the modulated-autocorrelations-drive shown in orange in Figure 3D. So the peak vanishes in the sum of all contributions to  $\delta c(t)$ . We will see in the next section that this scenario will change in the case of two homogeneously connected populations. In that case, the stationary parts of the pairwise correlations are positive, preventing the partly cancellation of the prefactor  $\overline{c} + \frac{1}{N}\overline{a}$ , which makes the  $S$ -terms small in the single population case.

For large noise, however, pairwise correlations are reduced also in the single population case. Thus the  $S$ -terms get more important, because the term  $\overline{c} + \frac{\overline{a}}{N}$  increases, but without acquiring dominance over the  $a$ -term (not shown).

Let us consider the case  $\omega = 0$  separately, because its analysis is easiest and due to the continuity of the observed quantities, it carries over to the case of small  $\omega$ , which are also the frequencies interesting for experimental reasons.

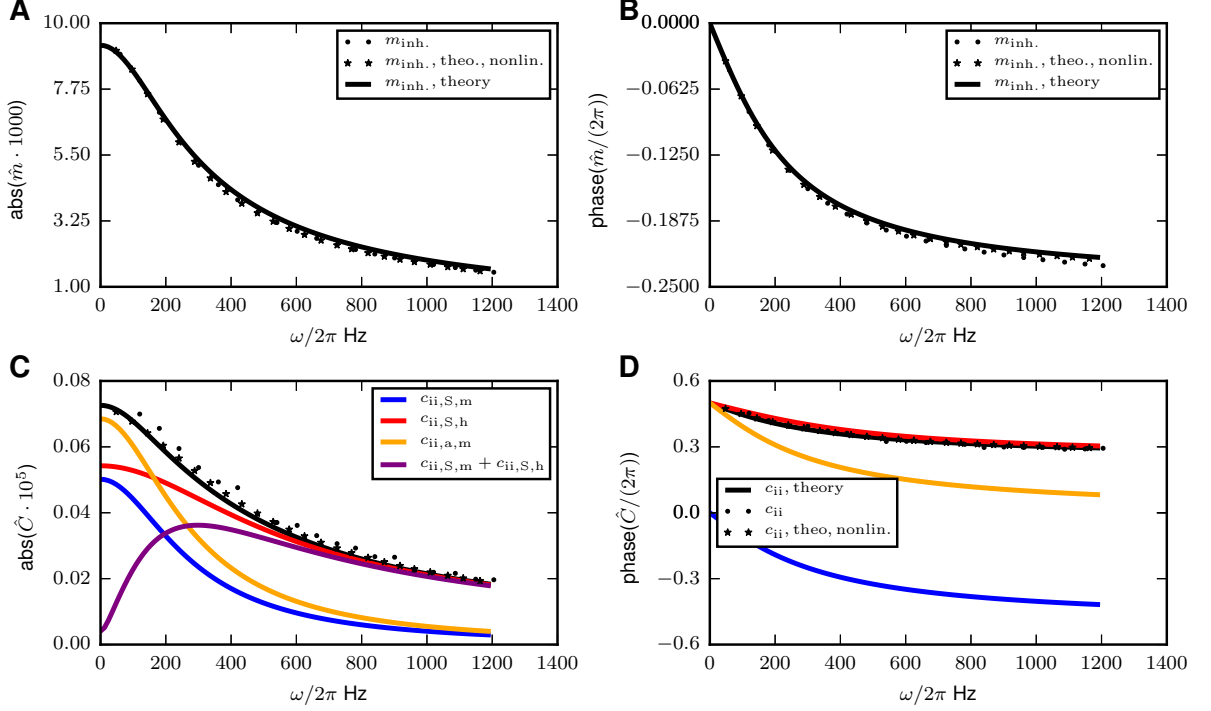


Figure 3. **Periodically driven single population network.** Dependence of the modulations of the mean activity (**A,B**) and correlations (**C,D**) on the driving frequency  $\omega$ : **A** Amplitude of modulation of mean activity. **B** Phase of modulation of mean activity relative to the external drive. **C** Amplitude of modulation of correlations. **D** Phase of modulation of correlation relative to the external drive. In all panels, the analytical predictions ((9) and (31)) are shown as full curves, numerical solutions of the full mean-field equations ((5) and (6)) by stars, and simulation results by dots. In panels **C** and **D**, the different contributions to the time-dependent correlations, identified in (11), are shown separately: The  $S_h$ -term in red, the  $S_m$ -term in blue, their sum in purple, and the  $a$ -term in yellow. Same color code used in D. The numerical results are obtained by using the integrate.ode-method from the python-package scipy [32] with the option “lsoda”, meaning that either implicit Adams- or backward differentiation-algorithms (depending on the given problem) are used. Network parameters: Number of neurons  $N_I = 5000$ , connection probability  $p_{II} = 0.1$ , coupling strength  $J_{II} = -1$ , mean activity  $m_I \approx 0.3$ , and  $\sigma_{\text{noise}} = \sigma_{\text{system}} := \sqrt{J_{II}^2 p_{II} N_I m_I (1 - m_I)} \approx 10.2$ .

Here, the  $S_m$ -term contributes with phase 0, because  $\bar{c} + \frac{\bar{a}}{N} > 0$ ,  $\delta m(t)$  is in phase with the perturbation and is multiplied by  $KJ < 0$  (which is negative, because neurons are inhibitory) and  $\frac{\partial S}{\partial \mu} KJ$  (negative as long as  $m_I < \frac{1}{2}$ , which is the realistic case studied here) and the solution  $\delta c(t)$  has the same sign as the inhomogeneity, because  $W < 0$ . The  $S_h$ -term is in anti-phase, because there  $KJ\delta m$  is replaced by  $h_{\text{ext}}$ , i.e. the direct, positive drive. Again because of  $W < 0$ , the  $a$ -term is in anti-phase as long as  $m_0 < \frac{1}{2}$ . For larger  $\omega$ , the phase lag is increasingly negative, because of the leak and the inhibitory feedback in the ODE (5).

#### Two populations, homogeneously connected

A slightly more realistic, but still simple setup is an EI-network with the same input for the inhibitory and the excitatory neurons, as studied before, e.g. in [11, parameters, except  $m_X$  as in fig. (6) there]. Here, pairwise correlations can also be positive, preventing the cancellation with the autocorrelations in the  $S$ -terms, which makes it possible that the varying susceptibilities and not the varying autocorrelations determine the shape of the correlations for small  $\omega$ . In this case, the competition of the two  $S$ -terms, which have different signs, together with the influence of the  $a$ -term lead to a resonance. This can be seen in panel **C** of Figure 4, where the absolute value of the pairwise correlations between pairs of excitatory neurons is shown. We here focus on the correlations between excitatory neurons, because their activities are recorded from most often and also cell assemblies are normally assumed to consist of excitatory neurons.



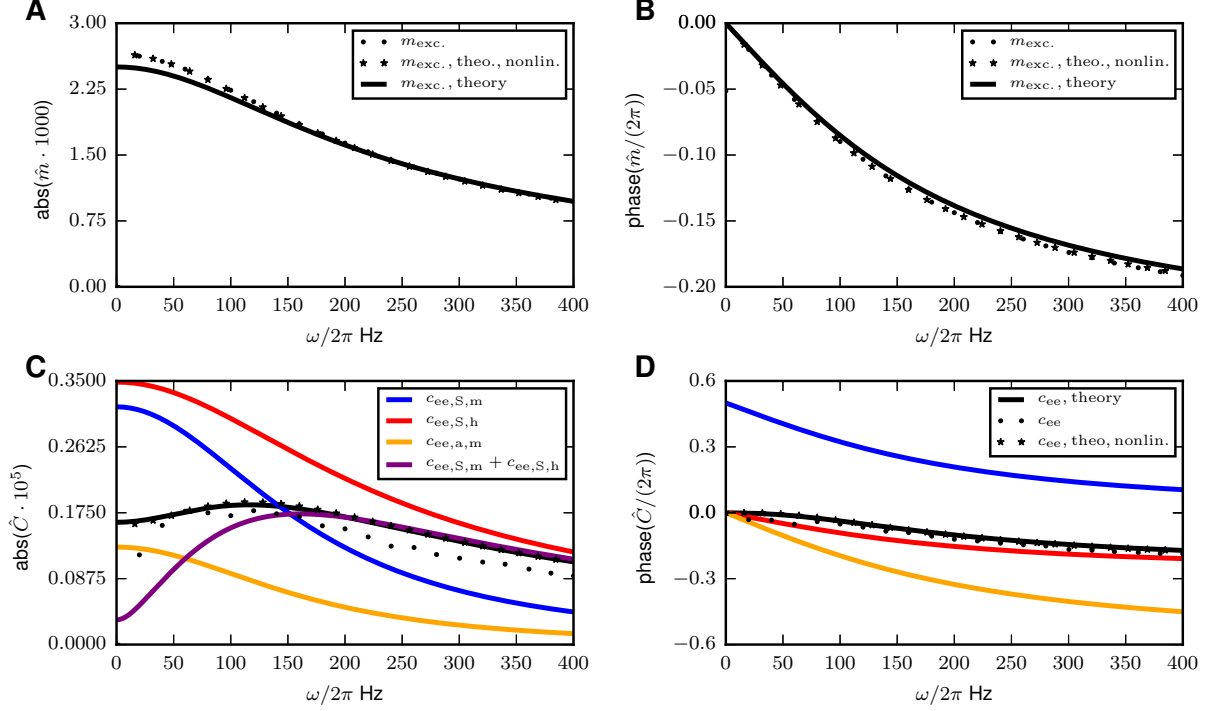


Figure 4. **Periodically driven E-I network.** **A** Amplitude of modulation of the mean activity deviating from the stationary value for the excitatory population. **B** Phase of the modulation of the mean activity. **C** Different contributions to the amplitude of pairwise correlation between pairs of excitatory cells in dependence of the frequency  $\omega$  of the external drive. **D** Phase of correlations relative to the driving signal. Analytical theory ((9), (31)) shown by solid curves, numerical solutions of the full mean field equations ((5) and (6)) (stars) and simulation results (dots). Same color code as in **C**. In **C** and **D**, the contributions to the variation of correlations are shown separately: The  $S_h$ -term in red, the  $S_m$ -term in blue, their sum in purple and the  $a$ -term in yellow. The legend for **C** and **D** is split over both panels. Numerical solutions obtained by the same methods as in Figure 3. Parameters:  $N_E = N_I = N_X = 8192$ ,  $p_E = p_I = p_X = p = 0.2$ ,  $m_E = m_I \approx 0.11$ ,  $m_X = 0.25$ , c.f. [11, e.g. fig. 6].

#### Two populations with inhomogeneous connections

In order to check if the theory also works for parameters satisfying biological constraints, we choose the connectivity and activity levels in accordance to experimental studies. Apart from the results from [8], the parameters were measured in the layer 2/3 in the barrel cortex of mice. We select this layer, because it is the assumed location of cell assemblies [33], allowing us to relate our results to the original hypothesis of excess synchrony by activation of assemblies [8], which is a feature that could be considered explicitly in future studies. The connection probabilities are taken from [34], the fractions of excitatory and inhibitory neurons from [35] and we extract the membrane time constant from [36, supplementary material]. We adjust the neurons' thresholds such that the stationarity condition  $\varphi(\bar{m}) = \bar{m}$  is fulfilled for  $m_\alpha = \tau\nu_\alpha$ , where  $\alpha \in \{\text{exc.}, \text{inh.}\}$ ,  $\nu_\alpha$  is the firing rate of the respective population and  $\tau$  is the neuronal time constant. Note that we identify the firing rate with  $\nu_\alpha = \frac{m_\alpha}{\tau}$  because  $\tau\nu_\alpha$  is the time a spiking neuron affects the downstream neurons. The identification of the transition  $0 \rightarrow 1$  with a spike would lead to the equation  $\nu_\alpha = \frac{m_\alpha(1-m_\alpha)}{\tau}$  [10]. We think, however, that this identification is inappropriate in our case, because the  $0 \rightarrow 1$ -transition for a binary neuron has a different meaning than a spike for a spiking neuron. In other words: If one wants to identify a spiking event for a binary neuron, one would have to count the  $1 \rightarrow 1$ -transition as spike as well. We take the ratio of the firing rates of inhibitory and excitatory neurons from [35] and, to get the rate for inhibitory neurons, scale with this ratio the rate of 18 Hz given in [8] that presumably reflects the activity of excitatory neurons (private communication). All parameters are summarized in Table I. The effective connectivity  $W$  of this system has two conjugate complex eigenvalues. Therefore, there exists a resonance frequency also for the mean activity (Figure 5).

In the two upper panels of Figure 5 and Figure 6, we have included the comparison of the stationary values for the mean activity (cf. (7)) and the correlations (cf. (8)), respectively with the time averaged results of the simulation and

		exc.	inh.	$\nu$ (Hz)	mean act.	#neurons	
exc.	connection prob.	0.168	0.5	18	0.045	1691	$\tau = 2.5$ ms
	synaptic weight	0.37	-0.52				
inh.	connection prob.	0.327	0.36	108	0.27	230	$m_{\text{ext}} = 0.1$
	synaptic weight	0.82	-0.54				

Table I. Parameters for the biologically inspired network model used in Figure 5, Figure 6, Figure 9 and Figure 10.

with the numerical solution of the full mean-field equations. The stationary statistics has been investigated before for other parameters in finite networks [11] and in the limit  $N \rightarrow \infty$  [13]. The second harmonics extracted from the simulations and the numerical solution of the full mean-field equations show good agreement on the one hand and on the other hand they are small compared to the zeroth and first harmonics, justifying the truncation of the Fourier series in the analytical theory after the first term.

The first harmonics of the mean activity (see Figure 5) and correlations (see Figure 6) predicted by the linear response theory agrees well with simulations and the numerical solution. This is not necessarily clear a priori because the perturbation in the input to every neuron is of the order  $\mathcal{O}(\frac{\sigma}{10})$ , where  $\sigma$  is the input noise level of the unperturbed system. However, linear response theory works surprisingly well, even for the correlations, where the perturbation is of the same order of magnitude as the stationary value. The maximal modulation in the firing rates amounts to  $\approx 0.8$  Hz for the excitatory and 4.9 Hz for the inhibitory neurons.

Because the connectivity matrix has complex eigenvalues  $\lambda_1 = \lambda_2^*$ , we observe a resonance of the mean activities at the frequencies

$$f_{\text{res,mean}} = \frac{\Im(\lambda_1)}{\tau 2\pi},$$

indicated in Figure 5C, by a vertical line. However, the components of  $\delta m$  are composed of different modes, therefore their maximum does not appear exactly at  $f_{\text{res,mean}}$ . For the correlations, we have more modes: In general, the correlation matrix for a three-dimensional quantity has 6 independent components. In our case,  $c_{XX}$  is always 0, which is a consequence of the missing feedback to  $X$ . Now, the evolution of every mode of  $\delta \tilde{c}$  is given by the sum of two eigenvalues of  $1 - W$ , i.e.  $2 - \lambda$ ,  $2 - \lambda^*$ ,  $2 - 2\lambda$ ,  $2 - 2\lambda^*$  and  $2 - (\lambda^* + \lambda)$ . The missing mode is the “trivial” one owing to the vanishing eigenvalue of  $W$ . So, the behavior of the “kernel” of the ODE for  $\delta c$  is given by the resonances at  $\frac{|\Im(\lambda)|}{\tau 2\pi}$  and  $2 \cdot \frac{|\Im(\lambda)|}{\tau 2\pi}$ . In addition, the inhomogeneity of the ODE (10) (its right hand side) is already resonant at  $\frac{|\Im(\lambda)|}{\tau 2\pi}$ . All these modes are mixed with different strength in the different modes of  $\delta c$ , giving rise to a maximum of  $|C_1|$  somewhere in the vicinity of  $f_{\text{res,mean}}$  and  $2f_{\text{res,mean}}$ . In all cases the “resonances” are damped, therefore, a resonance catastrophe, induced i.e. by  $\delta m$  oscillating with the resonance frequency of  $\delta c$ , cannot occur. We also notice that all resonances are the stronger, the closer  $\Re(\lambda)$  is to 1, i.e. the closer we are at the critical point, which makes sense intuitively: The damping comes from the inhibitory feedback. The stationary component has already been shown to correspond to the simulation [11], also confirmed here.

The  $\omega$ -dependencies of the  $c_{ii}$ - and the  $c_{ei}$ - correlations shown in the appendix are qualitatively similar ( Figure 9 and Figure 10).

Figure 7 illustratively summarizes the results of this section. In panel A, the probability of the binary system to be in a certain activity state  $(m_{\text{inh}}^0, m_{\text{exc}}^0)^T$  is indicated by different gray shades, the darker, the higher the probability to find the system in the respective area. On top, the border of the “ $\sigma$ -area” with maximally one standard deviation distance from the limit cycle, as it is predicted by the linear theory, is indicated by black dots. The construction of their locations is depicted in panel B: We draw the limit cycle (black) formed by the points  $(m_{\text{inh}}^0(t), m_{\text{exc}}^0(t))^T$  as a parametric plot with time as parameter. Then, we define the points on the error ellipse  $(m_{\text{inh}}, m_{\text{exc}})^T$  as follows

$$\delta \mathbf{m}(t)^T c^{\text{pop}}(t)^{-1} \delta \mathbf{m}(t) = 1, \quad (12)$$

where  $\delta \mathbf{m}^T := (m_{\text{inh}}, m_{\text{exc}}, 0)^T - (m_{\text{inh}}^0, m_{\text{exc}}^0, 0)^T$  and

$$c^{\text{pop}}(t) = \begin{pmatrix} c_{EE}^{\text{pop}}(t) & c_{EI}^{\text{pop}}(t) & c_{EX}^{\text{pop}}(t) \\ c_{EI}^{\text{pop}}(t) & c_{II}^{\text{pop}}(t) & c_{IX}^{\text{pop}}(t) \\ c_{EX}^{\text{pop}}(t) & c_{IX}^{\text{pop}}(t) & 0 \end{pmatrix}.$$

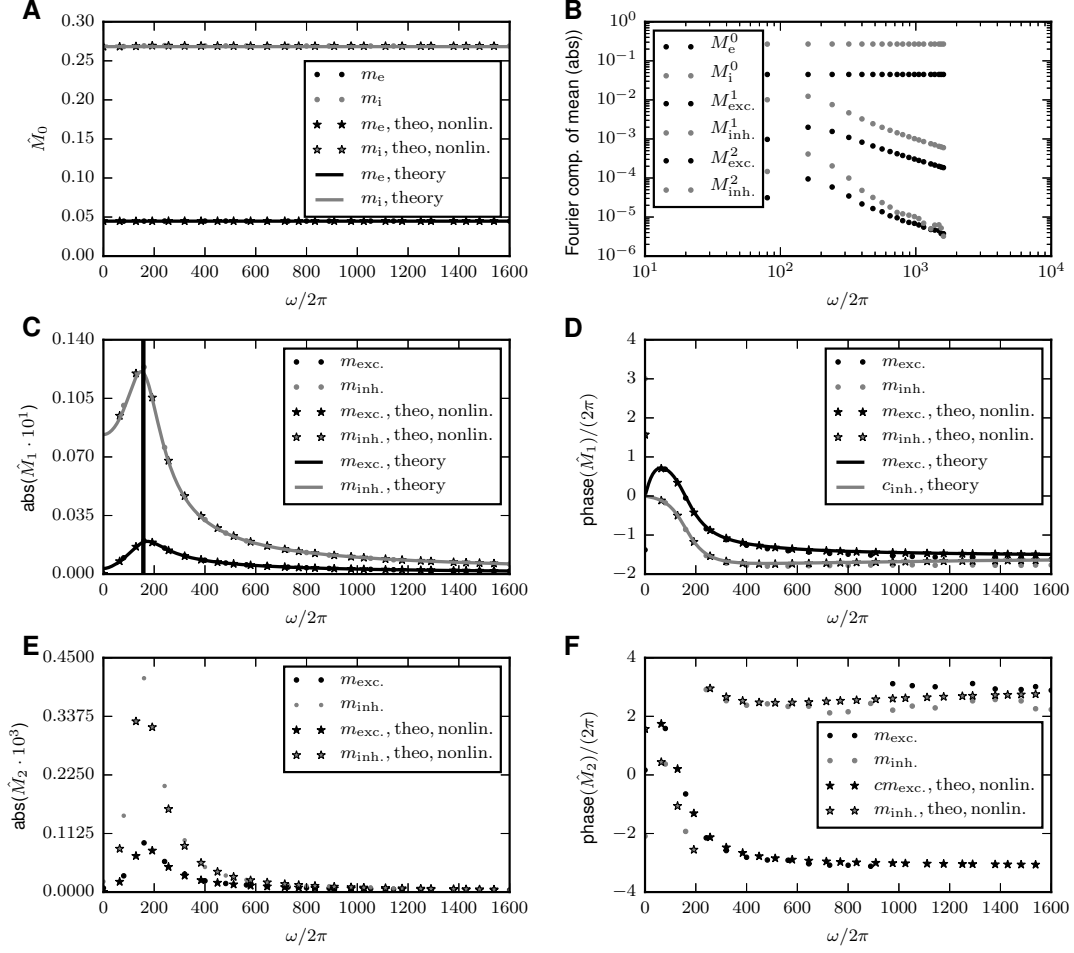


Figure 5. **Driven E-I network with biologically inspired parameters: Mean activity.** From the first to the third row, the zeroth to second order of the mean activity is shown. **A** Constant part of mean activity (zeroth order). **B** First three Fourier-modes of the mean activities on a loglog-scale. **C** Amplitude of first order of the mean activity. **D** Phase of first order relative to driving signal. **E** and **F** are structured analogous to **C** and **D** for the second Fourier modes. Solid curves indicate the linear theory ((9)), stars numerical integration of the full mean field equations ((5), (6)) and dots the simulation results of the full network. Black symbols indicate the activity of excitatory, gray symbols of inhibitory neurons. Numerical results obtained by the same methods as in Figure 3.  $\sigma_{\text{noise},E} = \sigma_{\text{noise},I} = 10$ ,  $\sigma_{\text{network},E} = 2.8$ ,  $\sigma_{\text{network},I} = 4.6$ , other parameters of the network model given in Table I.

The solutions  $\delta \mathbf{m}(t)$  of (12) are composed of all points that are one standard deviation away from the expected activity. The correlations enter the total population averaged variability given by

$$\begin{aligned}
 c_{\alpha\beta}^{\text{pop}}(t) &:= \langle \delta m_{\alpha}(t) \delta m_{\beta}(t) \rangle = \left\langle \frac{1}{N_{\alpha}} \sum_{i \in \alpha} \delta n_i(t) \frac{1}{N_{\beta}} \sum_{i \in \beta} \delta n_i(t) \right\rangle \\
 &= \frac{\delta_{\alpha\beta}}{N_{\alpha}^2} \sum_{i \in \alpha} \langle (\delta n_i(t))^2 \rangle + \frac{1}{N_{\alpha} N_{\beta}} \sum_{i \in \alpha, j \in \beta, i \neq j} \langle \delta n_i(t) \delta n_j(t) \rangle \\
 &\approx \delta_{\alpha\beta} \frac{a_{\alpha}(t)}{N_{\alpha}} + c_{\alpha\beta}(t)
 \end{aligned}$$

with the definitions (3) and (4).

The two points on the border of the dark gray error-ellipses of the full correlations with the biggest distance to the tangent of the limit cycle at  $(m_{\text{inh}}^0, m_{\text{exc}}^0)$  are marked by a star, which, taken together, form the border of the tube-shaped  $\sigma$ -area. This tube indicates the region in which we expect the system to be most likely. To visualize the contributions of auto- and pairwise correlations, we plot in light gray the error ellipses based solely on the auto

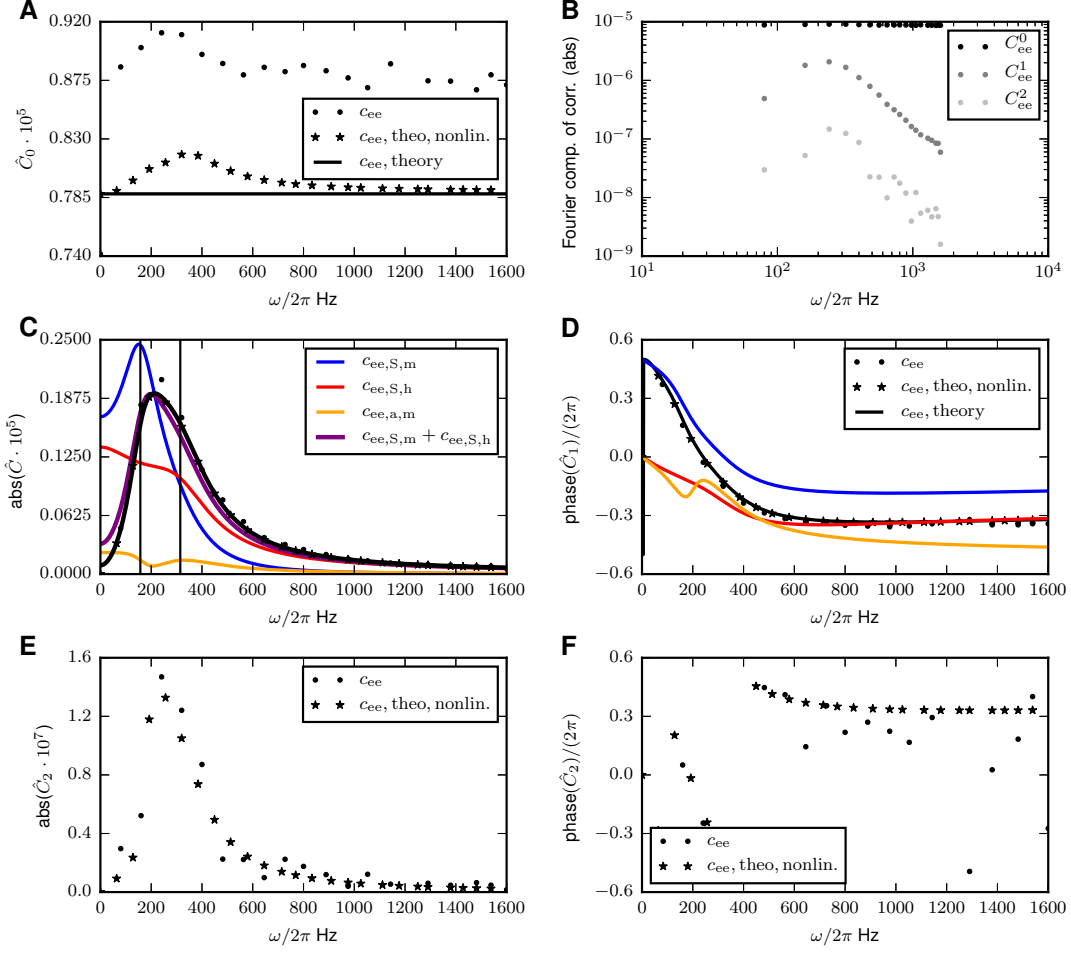


Figure 6. **Driven E-I network with biologically inspired parameters: EE-Covariance.** Response of the covariance to a perturbation with frequency  $\omega$  in the Fourier space. The first row (A) shows the zeroth order, i.e. the constant part, the second (C,D) and third rows (E,F) show the absolute value and the complex phase of the first and second Fourier coefficients. A Zeroth order (time independent part) of the covariance. B Absolute value of the first three Fourier components of the  $c_{ei}$ -correlations on a loglog-scale. C Absolute value of the first order of the time-dependent part of the covariance. D Phase angle in relation to the driving signal. E and F are structured analogous to C and D for the second Fourier modes. Solid lines indicate the linear theory (31), stars the results of the numerical solved full mean-field theory (5) and (6) and dots those of the direct simulation of the full network. Numerical results obtained by the same methods as in Figure 3. Parameters of the network model as in Figure 5.

correlations ( $c^{\text{pop}}(t)$  is diagonal in this case). The dark error ellipses are bigger than the light ones indicating that the pairwise correlations are positive and their axes are tilted, showing that the  $c_{EI} = c_{IE}$ -component is nonzero. Furthermore, the error ellipses significantly change their size in time, indicative of the modulation of the fluctuations with time. The autocorrelations grow monotonously with the respective mean activities, explaining that the light gray ellipses are largest (smallest) where the mean activities are largest (smallest). One can, for example, also read of the phase shift of  $c_{EE}$  to  $m_E$  of roughly  $\frac{\pi}{2}$  by the fact that the deviation of the dark gray error ellipses from the light gray ones is largest at the points where  $m_E(t) \approx \overline{m}_E$  and  $\delta m_I(t)$  is minimal.

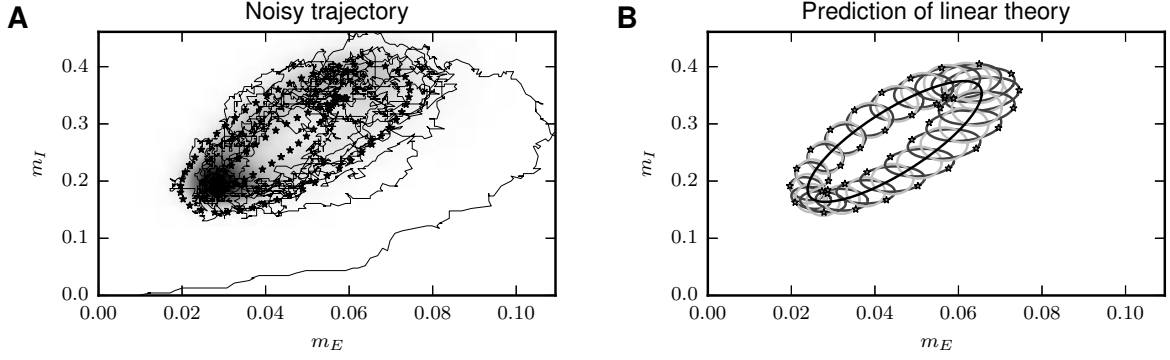


Figure 7. **Distribution of population-averaged activity of periodically driven E-I network.** **A** Empirical density of population activity of the E-I network. Gray shading indicates time-averaged occupation of states. The thin mid gray curve is a sample of the binary dynamics of 10 periods after the start of the simulation. The black dots indicate the  $\sigma$ -region predicted by the linear theory as described by (12) in the main text. **B** Limit cycle of the linear theory (black ellipse), together with error ellipses stemming from the sum of pairwise correlations and autocorrelations (dark gray, slightly tilted) and representing solely autocorrelations (light gray). The stars are at the same places as in (A). Parameters are given in Table I, only the perturbation strength is increased to  $h_{\text{ext}} = 6$  (noise level around 20) for reasons of readability (for this value the simulated results already show deviations from the linear approximation). The perturbing frequency is chosen to be  $f = 80$  Hz.

## METHODS

### Glauber dynamics in mean-field theory

We have left out so far several steps in the derivation of the results that were not necessary for the presentation of the main ideas. In this section, we will therefore give a self-contained derivation of our results also necessitating paraphrases of some results known from earlier works. Starting point is the master equation for the probability density of the possible network states emerging from the Glauber dynamics [28] described in (see for the following also [11, 29])

$$\frac{\partial p}{\partial t}(\mathbf{n}, t) = \underbrace{\frac{1}{\tau}}_{\text{update rate}} \sum_{i=1}^N \underbrace{(2n_i - 1)}_{\in \{-1, 1\}, \text{direction of flux}} \underbrace{\phi_i(\mathbf{n} \setminus n_i, t)}_{\text{net flux due to neuron } i} \quad \forall \quad \mathbf{n} \in \{0, 1\}^N, \quad (13)$$

where

$$\begin{aligned} \phi_i(\mathbf{n} \setminus n_i, t) &= \underbrace{p(\mathbf{n}_{i-}, t) F_i(\mathbf{n}_{i-})}_{\text{neuron } i \text{ transition up}} - \underbrace{p(\mathbf{n}_{i+}, t) (1 - F_i(\mathbf{n}_{i+}))}_{\text{neuron } i \text{ transition down}} \\ &= -p(\mathbf{n}_{i+}) + p(\mathbf{n}_{i-}, t) F_i(\mathbf{n}_{i-}) + p(\mathbf{n}_{i+}, t) F_i(\mathbf{n}_{i+}). \end{aligned}$$

The activation function  $F_i(\mathbf{n})$  is given by (1).

Using the master equation (for details cf. appendix, ), one can derive a differential equation for the mean activity of the neuron  $i$ ,  $\langle n_i \rangle(t) = \sum_{\mathbf{n}} p(\mathbf{n}, t) n_i$  and the raw correlation of the neurons  $i$  and  $j$ ,  $\langle n_i n_j \rangle(t) = \sum_{\mathbf{n}} p(\mathbf{n}, t) n_i n_j$  [9, 11, 13, 28, 29]. This yields

$$\begin{aligned} \tau \frac{d}{dt} \langle n_k \rangle(t) &= -\langle n_k \rangle(t) + \langle F_k(t) \rangle \\ \frac{d}{dt} \langle n_k(t) n_l(t) \rangle &= \{-\langle n_k(t) n_l(t) \rangle + \langle n_l(t) F_k(t) \rangle\} + \{k \leftrightarrow l\}. \end{aligned} \quad (14)$$

As mentioned in , we assume that the input  $h_i$  coming from the local and the external population is normally

distributed, say with mean  $\mu_i$  and standard deviation  $\sigma_i$  given by

$$\begin{aligned}\mu_i &:= \langle h_i \rangle = (J \langle \mathbf{n} \rangle)_i + h_{\text{ext}} \sin(\omega t) \\ \sigma_i^2 &:= \langle h_i^2 \rangle - \langle h_i \rangle^2 = \sum_{k,k'=1}^N J_{i,k} J_{i,k'} (\langle n_k n_{k'} \rangle - \langle n_k \rangle \langle n_{k'} \rangle) + (\sigma_i^{\text{noise}})^2 \\ &= (J^T c J)_{ii} + J \otimes J \langle \mathbf{n} \rangle \otimes (1 - \langle \mathbf{n} \rangle) + (\sigma_i^{\text{noise}})^2,\end{aligned}\tag{15}$$

where the average  $\langle \rangle$  is taken over realizations of the stochastic dynamics and we introduced the element-wise (Hadamard) product of two matrices  $A, B$  [see 37, for a consistent notation of matrix operations]

$$(A \otimes B)_{ij} := A_{ij} B_{ij}.\tag{16}$$

The additional noise introduced in (1) effectively leads to a smoothing of the neurons' activation threshold and broadens the width of the input distribution. It can be interpreted as additional variability coming from other brain areas. Furthermore, it is computationally convenient, because the theory assumes the input to be a (continuous) Gaussian distribution, while in the simulation, the input  $\sum_{l=k}^N J_{ik} n_k$ , being a sum of discrete binary variables, can only assume discrete values. The smoothing by the additive noise therefore improves the agreement of the continuous theory with the discrete simulation. Already weak external noise compared to the intrinsic noise is sufficient to obtain a quite smooth probability distribution of the input, cf. Figure 8.

The description in terms of a coupled set of moment equations instead of the ODE for the full probability distribution here serves to reduce the dimension: It is sufficient to describe the time evolution of the moments on the population level, rather than on the level of individual units. To this end we need to assume that the synaptic weights  $J_{ij}$  only depend on the population  $\alpha, \beta \in \{exc., inh., ext.\}$  that  $i$  and  $j$  belong to, respectively, and thus (re)name them  $J_{\alpha\beta}$  (homogeneity). Furthermore, we assume that not all neurons are connected to each other, but that  $K_{\alpha\beta}$  is the number of incoming connections a neuron in population  $\alpha$  receives from a neuron in population  $\beta$  (fixed in-degree). The incoming connections to each neuron are chosen randomly, uniformly distributed over all possible sending neurons. This leads to expressions for the population averaged input  $h_\alpha$ , mean activity  $m_\alpha$  and pairwise correlation  $c_{\alpha\beta}$ , formally nearly identical to those on the single cell level and analogous to those in [11, sec. Mean-field solution].

*Mean activity: Stationary part and response to perturbation in linear order*

We are now able to calculate the quantity  $\langle F_\alpha(\mathbf{n}(t), t) \rangle = \langle H(h_\alpha(t) - \theta) \rangle$  (recall that  $h_\alpha(t)$  is a Gaussian random variable with mean  $\mu_\alpha(t)$  and standard deviation  $\sigma_\alpha(t)$ ), the nonlinearity of the ODEs (14) on the population level. Multiplying  $H(x_\alpha(t) - \theta_\alpha)$  by the Gaussian probability density for  $x_\alpha(t)$ , we get, after substitution of the integration variable,

$$\begin{aligned}\langle F_\alpha(\mathbf{n}(t), t) \rangle &= \langle H(x_\alpha(t) - \theta_\alpha) \rangle \\ &= \frac{1}{\sqrt{\pi}} \int_{\frac{\theta - \mu_\alpha(t)}{\sqrt{2}\sigma_\alpha(t)}}^\infty e^{-x^2} dx = \frac{1}{2} \text{erfc}\left(\frac{\theta_\alpha - \mu_\alpha(t)}{\sqrt{2}\sigma_\alpha(t)}\right) \\ &=: \varphi(\mu_\alpha(\mathbf{m}(t), c(t), h_{\text{ext}} \sin(\omega t)), \sigma_\alpha(\mathbf{m}(t), c(t))),\end{aligned}\tag{17}$$

where we defined the average input  $\mu_\alpha$  and the width of the input distribution  $\sigma_\alpha$

$$\mu_\alpha(t) := [(K \otimes J) \mathbf{m}(t)]_\alpha + h_{\text{ext}} \sin(\omega t)\tag{18}$$

$$\begin{aligned}\sigma_\alpha^2(t) &:= [(K \otimes J)^T c(t) (K \otimes J)]_{\alpha\alpha} \\ &\quad + [K \otimes J \otimes J \mathbf{m}(t) \otimes (1 - \mathbf{m}(t))]_\alpha + \sigma_{\alpha, \text{noise}}^2.\end{aligned}\tag{19}$$

Recall that we defined  $\bar{x}$  to be the quantity  $x$  in the stationary case (without external input). For the linear approximation around  $\mu_\alpha = \bar{\mu}_\alpha$ ,  $\sigma_\alpha = \bar{\sigma}_\alpha$  and  $h_{\text{ext}} = 0$ , we have to take into account all dependencies via inner derivatives. We set  $\delta\mu_\alpha = \mu_\alpha - \bar{\mu}_\alpha$  and  $\delta\sigma_\alpha = \sigma_\alpha - \bar{\sigma}_\alpha$ . Note that  $\delta\mu$  includes the variation of  $\mu$  both because of fluctuations in the network and because of the external drive. The Taylor expansion up to linear order is

$$\varphi(\mu_\alpha(\mathbf{m}, c), h_0, \sigma_\alpha(\mathbf{m}, c)) \approx \underbrace{\varphi(\bar{\mu}_\alpha, \bar{\sigma}_\alpha)}_{=: \bar{S}_\alpha} + \bar{S}_\alpha \left[ \delta\mu_\alpha + \frac{\theta - \bar{\mu}_\alpha}{\bar{\sigma}_\alpha} \delta\sigma_\alpha \right],$$



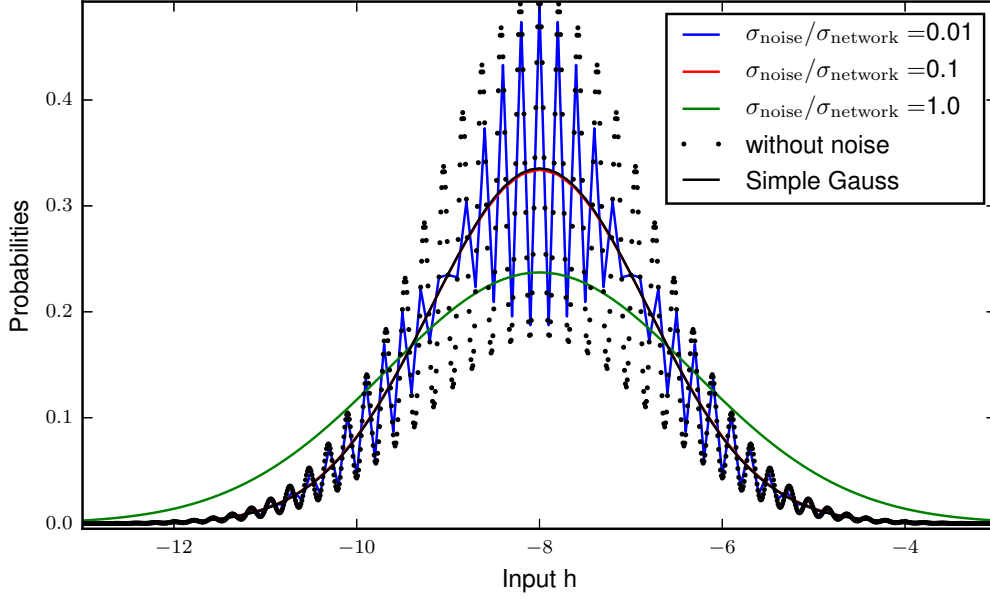


Figure 8. **Distribution of inputs from binary neurons for different noise levels:** Probability distribution of synaptic input  $h_i = \sum_j J_{ij} n_j + \xi$  of a neuron in a network of independently active cells  $n_j$  with  $\langle n_E \rangle = \langle n_I \rangle = 0.2$  and synaptic weights  $j_I = -0.21$ ,  $j_E = 0.01$ .  $\left| \frac{j_E}{j_I} \right|$  was deliberately chosen to be large because only then the convolution of a binomial distribution “squeezed” to the step size  $j_E$  with the binomial distribution squeezed only to the step size  $|j_I|$  results in a probability distribution with many local maxima leading to the impression of an oscillation. Noiseless case  $\xi = 0$  shown as black dots. The solid black curve indicates the Gaussian approximation (cf. e.g. (15), here without perturbation) of this distribution from the main text. This distribution appears in the expectation values of the activation function  $F$  (cf. e.g. (1)): Is a Gaussian distribution with the mean  $\mu = K_E j_E m_E + K_I j_I m_I$  and the variance  $\sigma_{\text{network}}^2 = K_E j_E^2 m_E (1 - m_E) + K_I j_I^2 m_I (1 - m_I)$  of the original binomial distributions  $\text{Binom}(m_E, K_E)$ ,  $\text{Binom}(m_I, K_I)$ . The other curves indicate convolutions with the Gaussian noise  $\xi \sim \mathcal{N}(0, \sigma_{\text{noise}})$  of different magnitudes  $\sigma_{\text{noise}}$ , given in units of the noise level  $\sigma_{\text{network}}$  intrinsically produced by the network.

where we introduced the susceptibility on the population level

$$S(\mu_\alpha(t), \sigma_\alpha(t)) := \frac{d}{d\mu_\alpha(t)} \varphi(\mu_\alpha(t), \sigma_\alpha(t)) = \frac{1}{\sqrt{2\pi}\sigma_\alpha(t)} e^{-\frac{(\mu_\alpha(t) - \theta_\alpha)^2}{2\sigma_\alpha^2(t)}}. \quad (20)$$

Now, we express  $\delta\sigma_\alpha$  and  $\delta\mu_\alpha$  via  $\delta\mathbf{m} := \mathbf{m} - \overline{\mathbf{m}}$  (cf. [11, eq. (29)] for the time-independent case):

$$\begin{aligned} \delta\mu_\alpha(t) &= \sum_\beta K_{\alpha\beta} J_{\alpha\beta} \delta m_\beta(t) + h_{\text{ext}} \sin(\omega t) \\ \delta\sigma_\alpha(t) &= \frac{1}{2\sigma_\alpha} \left( \sum_\beta K_{\alpha\beta} J_{\alpha\beta}^2 (1 - 2m_\beta) \delta m_\beta(t) + \sum_{\beta, \gamma} K_{\alpha\beta} K_{\alpha\gamma} J_{\alpha\beta} J_{\alpha\gamma} \delta c_{\beta\gamma}(t) \right). \end{aligned} \quad (21)$$

Note that in  $\delta\mu_\alpha$  (but not  $\delta\sigma_\alpha$ ), the perturbation occurs again explicitly. We will see later ((31) and discussion thereafter) that  $\delta c$  scales like  $\frac{\delta m}{N}$ . Furthermore, we have certainly  $\frac{|K|}{N} = \mathcal{O}(1)$  and  $\sigma = \mathcal{O}(\sqrt{|K|})$ , thus

$$|\delta\boldsymbol{\mu}(t)| = \mathcal{O}(|K| |\delta\mathbf{m}(t)|) = \mathcal{O}(h_{\text{ext}}), \text{ but } |\delta\boldsymbol{\sigma}(t)| = \mathcal{O}(\sqrt{|K|} |\delta\mathbf{m}(t)|) = \mathcal{O}\left(\frac{h_{\text{ext}}}{\sqrt{|K|}}\right).$$

The Gaussian closure implies the neglect of terms of order  $\sqrt{|K|}$ , therefore we must set  $\delta\boldsymbol{\sigma}$  to zero in our calculations

to stay consistent. This yields for the linearization of the ODE (5)

$$\begin{aligned} \tau \frac{\partial}{\partial t} \delta m_\alpha(t) + \delta m_\alpha(t) &= \bar{S}_\alpha \left[ \delta \mu_\alpha(t) + \underbrace{\frac{\theta_\alpha - \bar{\mu}_\alpha}{\bar{\sigma}_\alpha}}_{=\text{erfc}^{-1}(\bar{m})} \delta \sigma_\alpha(t) \right] \\ \tau \frac{\partial}{\partial t} \delta m_\alpha(t) + \delta m_\alpha(t) &\approx \sum_\beta W_{\alpha\beta} \delta m_\beta(t) + \bar{S}_\alpha h_{\text{ext}} \sin(\omega t), \end{aligned} \quad (22)$$

where we used the relation  $\frac{\theta_\alpha - \bar{\mu}_\alpha}{\bar{\sigma}_\alpha} = \sqrt{2} \text{erfc}^{-1}(2\bar{m}_\alpha)$ , derived from (7) in connection with (17), which implies that this expression does not depend on  $K$ , but solely on  $m_\alpha$  and we defined

$$W_{\alpha\beta} := \bar{S}_\alpha K_{\alpha,\beta} J_{\alpha,\beta}.$$

The only change compared to the setup in [11] is again the occurrence of a periodical term, here  $S_\alpha h_{\text{ext}} \sin(\omega t)$ .

We solve (22) by transforming it into the eigenbasis of the matrix  $W_{\alpha,\beta}$

$$U^{-1} W U = \text{diag}(\lambda_1, \dots, \lambda_{\bar{N}}) := \Lambda. \quad (23)$$

We multiply (22) by  $U^{-1}$ , define  $\delta m^\alpha := (U^{-1})^{\alpha\beta} \delta m_\beta$  and get

$$\tau \frac{d}{dt} \delta m^\alpha = -\delta m^\alpha + \Lambda_\beta^\alpha \delta m^\beta + (U^{-1})^{\alpha\beta} \bar{S}_\beta h_{\text{ext}} \sin(\omega t). \quad (24)$$

Note that the noise is projected onto the respective eigenmodes. (24) can be solved including the transient phase by the method of variation of constants.

But as we are only interested in the cyclostationary part of the solution, we can neglect the solution of the homogeneous part and only compute the particular solution. Observe that  $\frac{d}{dt} \text{Im}(\delta m^\alpha(t)) = \text{Im}\left(\frac{d}{dt} \delta m^\alpha(t)\right)$  for a differentiable function  $\delta m^\alpha$  because  $t \in \mathbb{R}$ . We insert the ansatz  $\delta m^\alpha = M_1^\alpha e^{i\omega t}$  and solve for  $M_1^\alpha$ , which gives (9) of the main text. For further calculations, keep in mind that  $M_1^\alpha$  and therefore  $\delta m_\alpha$  are of order  $\mathcal{O}\left(h_{\text{ext}} \frac{S}{SKJ}\right) = \mathcal{O}\left(h_{\text{ext}} \frac{1}{KJ}\right)$ . In the appendix, we describe how to extract the right phase of the real solution from the complex ansatz.

#### Pairwise correlations: Stationary part and response to a perturbation in linear order

Using (14) in the population-averaged version, we calculate the derivative of the zero time-lag correlation

$$c_{\alpha\beta}(t) := \frac{1}{N_\alpha N_\beta} \sum_{i \in \alpha, j \in \beta, i \neq j} \langle n_i(t) n_j(t) \rangle - \langle n_i(t) \rangle \langle n_j(t) \rangle$$

getting

$$\tau \frac{dc_{\alpha\beta}(t)}{dt} = -2c_{\alpha\beta}(t) + \frac{1}{N_\alpha N_\beta} \sum_{i \in \alpha, j \in \beta, i \neq j} \langle F_j(\mathbf{n}(t)) \delta n_i(t) \rangle + \langle F_i(\mathbf{n}(t)) \delta n_j(t) \rangle.$$

Neglecting cumulants of order higher than two, we can expand the expectation value  $\langle F_i(\mathbf{n}(t)) \delta n_j(t) \rangle$  (cf. [11, 27, section "Linearized equation for correlations and susceptibility"]) and get

$$\langle F_i(\mathbf{n}(t)) \delta n_j(t) \rangle \approx \sum_{k \neq j} S(\mu_i(t), \sigma_i(t)) J_{ik} c_{kj}(t) + S(\mu_i(t), \sigma_i(t)) J_{ij} a_j(t). \quad (25)$$

After carrying out the population averaging, we get the ordinary differential equation

$$\begin{aligned} \tau \frac{dc_{\alpha\beta}(t)}{dt} &= \left\{ -c_{\alpha\beta}(t) + \sum_\gamma S(\mu_\alpha(t), \sigma_\beta(t)) K_{\alpha\gamma} J_{\alpha\gamma} \left( c_{\gamma\beta}(t) + \delta_{\gamma\beta} \frac{a_\beta(t)}{N_\beta} \right) \right\} + \{\alpha \leftrightarrow \beta\}. \end{aligned}$$

Therefore, the stationary part  $\bar{c}$  of the correlations fulfills the relation (cf. [11, 27])

$$2\bar{c}_{\alpha\beta} = \sum_{\gamma} S(\bar{\mu}_{\alpha}, \bar{\sigma}_{\alpha}) (K \circ J)_{\alpha\gamma} \left( \bar{c}_{\gamma\beta} + \delta_{\gamma\beta} \frac{\bar{a}_{\beta}}{N_{\beta}} \right) + \alpha \leftrightarrow \beta. \quad (26)$$

As for the mean activities, we want to make a little step (of order  $h_{\text{ext}}$ , to be precise) away from the stationary state determining the deviation  $\delta c(t) := c(t) - \bar{c}$ . For that, we have to calculate the Taylor expansion of  $S(\mu_{\alpha}(t), \sigma_{\alpha}(t))$  in  $\delta m$ , i.e.

$$\begin{aligned} & S(\mu_{\alpha}(t), \sigma_{\alpha}(t)) \\ &:= \frac{1}{\sqrt{2\pi}} \frac{1}{\sigma_{\alpha}(t)} \exp\left(-\frac{(\mu_{\alpha}(t) - \theta_{\alpha})^2}{2(\sigma_{\alpha}(t))^2}\right) \\ &\approx S(\bar{\mu}_{\alpha}, \bar{\sigma}_{\alpha}) + \left( \frac{\partial S}{\partial \mu_{\alpha}(t)} \delta \mu_{\alpha} + \frac{\partial S}{\partial \sigma_{\alpha}(t)} \delta \sigma_{\alpha} \right) \Big|_{\mu_{\alpha}=\bar{\mu}_{\alpha}, \sigma_{\alpha}=\bar{\sigma}_{\alpha}}, \end{aligned}$$

where  $\delta \mu_{\alpha}$  and  $\delta \sigma_{\alpha}$  are given by (21) and

$$\begin{aligned} \frac{\partial S}{\partial \mu_{\alpha}(t)}(\bar{\mu}_{\alpha}, \bar{\sigma}_{\alpha}) &= S(\bar{\mu}_{\alpha}, \bar{\sigma}_{\alpha}) \underbrace{\frac{(\theta_{\alpha} - \bar{\mu}_{\alpha})}{(\bar{\sigma}_{\alpha})^2}}_{=\mathcal{O}\left(\frac{1}{\sqrt{K}}\right)} \\ \frac{\partial S}{\partial \sigma_{\alpha}(t)}(\bar{\mu}_{\alpha}, \bar{\sigma}_{\alpha}) &= S(\bar{\mu}_{\alpha}, \bar{\sigma}_{\alpha}) \underbrace{\frac{(\theta_{\alpha} - \bar{\mu}_{\alpha})}{(\bar{\sigma}_{\alpha})^2}}_{=\mathcal{O}\left(\frac{1}{\sqrt{K}}\right)} \left( \underbrace{\frac{(\theta_{\alpha} - \bar{\mu}_{\alpha})}{\bar{\sigma}_{\alpha}}}_{=\mathcal{O}(1)} - \underbrace{\frac{\bar{\sigma}_{\alpha}}{(\theta_{\alpha} - \bar{\mu}_{\alpha})}}_{=\mathcal{O}(1)} \right) \end{aligned}$$

Here again, the relation  $\frac{\theta_{\alpha} - \bar{\mu}_{\alpha}}{\bar{\sigma}_{\alpha}} = \sqrt{2} \text{erfc}^{-1}(2\bar{m}_{\alpha})$  was used. We insert the linearization of  $S$  and the expressions for  $\delta \mu$  and  $\delta \sigma$ , (21), into the ODE for  $c_{\alpha\beta}(t) = \bar{c}_{\alpha\beta} + \delta c_{\alpha\beta}(t)$  to get after neglecting the contributions of order  $\mathcal{O}(h_{\text{ext}}^2)$  and sorting the rest into terms proportional to  $\delta c$ ,  $h_0$  and  $\delta m$  respectively:

$$\begin{aligned} & \tau \frac{d}{dt} \delta c_{\alpha\beta}(t) + \left\{ \sum_{\gamma} (\delta_{\alpha\gamma} - S(\bar{\mu}_{\alpha}, \bar{\sigma}_{\alpha}) K_{\alpha\gamma} J_{\alpha\gamma}) \delta c_{\gamma\beta}(t) \right\} + \{\alpha \leftrightarrow \beta\} \\ &= \left\{ \frac{\partial S}{\partial \mu_{\alpha}(t)} \sum_{\gamma} K_{\alpha\gamma} J_{\alpha\gamma} \left( \bar{c}_{\gamma\beta} + \frac{\bar{a}_{\beta}}{N_{\beta}} \delta_{\gamma\beta} \right) \left( h_{\text{ext}} \sin(\omega t) + \underbrace{\sum_{\delta} K_{\alpha\delta} J_{\alpha\delta} \delta m_{\delta}(t)}_{=\mathcal{O}(h_{\text{ext}})} \right) \right. \\ & \quad + \frac{\partial S}{\partial \sigma_{\alpha}(t)} \sum_{\gamma} K_{\alpha\gamma} J_{\alpha\gamma} \left( \bar{c}_{\gamma\beta} + \frac{\bar{a}_{\beta}}{N_{\beta}} \delta_{\gamma\beta} \right) \underbrace{\delta \sigma_{\alpha}(t)}_{=\mathcal{O}\left(\frac{h_{\text{ext}}}{\sqrt{K}}\right)} \\ & \quad \left. + S(\bar{\mu}_{\alpha}, \bar{\sigma}_{\alpha}) K_{\alpha\beta} J_{\alpha\beta} \frac{(1 - 2\bar{m}_{\beta})}{N_{\beta}} \delta m_{\beta}(t) \right\} + \{\alpha \leftrightarrow \beta\} \end{aligned} \quad (27)$$

As noted above, the third line in (27) is of order  $\frac{1}{\sqrt{K}}$  compared to the other contributions. Consequently, we neglect this part to stay consistent with the analysis for  $\delta m$ . Defining

$$\begin{aligned} T_{\alpha\beta} &:= K_{\alpha\beta} J_{\alpha\beta} \\ V_{\alpha\beta} &:= \frac{\theta_{\alpha} - \bar{\mu}_{\alpha}}{(\bar{\sigma}_{\alpha})^2} S(\bar{\mu}_{\alpha}, \bar{\sigma}_{\alpha}) K_{\alpha\beta} J_{\alpha\beta}, \end{aligned} \quad (28)$$

and

$$\begin{aligned}
N_{\alpha\beta}^{\text{diag}} &= \delta_{\alpha\beta} N_{\alpha} \\
\overline{m}_{\alpha\beta}^{\text{diag}} &= \delta_{\alpha\beta} \overline{m}_{\alpha} \\
\overline{a}_{\alpha\beta}^{\text{diag}} &= \delta_{\alpha\beta} \overline{a}_{\alpha} \\
\delta m_{\alpha\beta}^{\text{diag}}(t) &= \delta_{\alpha\beta} \delta m_{\alpha}(t) \\
(T\delta m(t))_{\alpha\beta}^{\text{diag}} &= \delta_{\alpha\beta} \sum_{\gamma} T_{\alpha\gamma} \delta m_{\gamma}(t),
\end{aligned} \tag{29}$$

we end up with the index-free version (10). The first two inhomogeneities, from now termed susceptibility terms represent the nonlinearity of the gain-function. Note that

$$\underbrace{(T\delta m)^{\text{diag}}}_{=\mathcal{O}(h_{\text{ext}})} + \underbrace{h_{\text{ext}} \sin(\omega t)}_{=\mathcal{O}(h_{\text{ext}})} = \left(\overline{S}^{\text{diag}}\right)^{-1} \left(\tau \frac{\partial}{\partial t} \delta m + \delta m\right) = \mathcal{O}\left(\sqrt{|K|} |\delta m|\right) = \mathcal{O}\left(\frac{h_{\text{ext}}}{\sqrt{|K|}}\right). \tag{30}$$

Thus, every of the two susceptibility terms separately is of order  $\sqrt{K}$  bigger than their sum. Furthermore

$$\mathcal{O}(V) = \mathcal{O}\left(\frac{1}{\sigma} \frac{\Theta - \mu}{\sigma} W\right) = \mathcal{O}\left(\frac{1}{\sqrt{K}} W\right),$$

which shows that the sum of the susceptibility terms are of the same order of magnitude with respect to its dependence on  $K$ , i.e. the connection probabilities and the system size, namely  $\mathcal{O}\left(\frac{h_{\text{ext}} W}{K}\right)$ , as the term coming from the time modulation of the autocorrelations (modulated-autocorrelations-drive), which is indeed of the order  $W\delta m = \mathcal{O}\left(\frac{h_{\text{ext}} W}{K}\right)$ . The fact that the sum of both susceptibility terms is smaller than the two summands shows especially that they have opposite signs reflecting that the direct drive represents the direct input  $h_{\text{ext}} \sin(\omega t)$  and the recurrent drive represents the effectively inhibitory response of the network (the matrix  $T$  has only non-positive eigenvalues).

With  $U$  given in (23), we multiply (27) from the left by  $U^{-1}$  and from the right by  $(U^{-1})^T$  to get (cf. [11, 27])

$$\begin{aligned}
&\tau \frac{d}{dt} \underbrace{U^{-1} \delta c(t) (U^{-1})^T}_{:=\widetilde{\delta c}} \\
&= \left\{ (-\mathbb{1} + \underbrace{U^{-1} W U}_{=\Lambda}) \underbrace{U^{-1} \delta c(t) (U^{-1})^T}_{:=\delta c(t)} \right. \\
&\quad + U^{-1} \left( (T\delta m(t))^{\text{diag}} + h_{\text{ext}} \sin(\omega t) \right) V \left( \overline{c} + \frac{1}{N^{\text{diag}}} \overline{a}^{\text{diag}} \right) (U^{-1})^T \\
&\quad + U^{-1} W (\mathbb{1} - 2\overline{m}^{\text{diag}}) \frac{1}{N^{\text{diag}}} \delta m(t)^{\text{diag}} (U^{-1})^T \Big\} \\
&\quad + \{\dots\}^T.
\end{aligned}$$

We are only interested in the cyclostationary statistics, so we can ignore again the transient state making the ansatz  $\widetilde{\delta c_{\alpha\beta}^{\text{inhom}}} = \widetilde{C_{\alpha\beta}^1} e^{i\omega t}$ . Inserting this and transforming back into the original system, we get

$$C_{\alpha\beta}^1 = h_{\text{ext}} \frac{-i\tau\omega + 2 - (\lambda_{\alpha} + \lambda_{\beta})}{(\tau\omega)^2 + (2 - (\lambda_{\alpha} + \lambda_{\beta}))^2} \left[ \sum_{\gamma, \delta, \theta, \phi, \eta} U_{\alpha, \eta}^{-1} U_{\beta, \delta}^{-1} T_{\eta, \theta} U_{\theta, \phi} (U^{-1} S)_{\phi} \frac{-i\tau\omega + 1 - \lambda_{\phi}}{(\tau\omega)^2 + (1 - \lambda_{\phi})^2} V_{\eta, \gamma} \left( \overline{c} + \frac{1}{N^{\text{diag}}} \overline{a}^{\text{diag}} \right)_{\gamma, \delta} \right. \tag{31}$$

$$+ \sum_{\gamma, \delta, \epsilon} U_{\alpha, \epsilon}^{-1} U_{\beta, \delta}^{-1} V_{\epsilon, \gamma} \left( \overline{c} + \frac{1}{N^{\text{diag}}} \overline{a}^{\text{diag}} \right)_{\gamma, \delta} \tag{32}$$

$$+ \sum_{\theta, \phi, \gamma} U_{\alpha, \gamma}^{-1} U_{\beta, \theta}^{-1} W_{\gamma, \theta} (1 - 2\overline{m}_{\theta}^{\text{diag}}) \frac{1}{N_{\theta}} U_{\theta, \phi} (U^{-1} S)_{\phi} \frac{-i\tau\omega + 1 - \lambda_{\phi}}{(\tau\omega)^2 + (1 - \lambda_{\phi})^2} \Big]$$

Together with (9), this is the main result of this section.

## DISCUSSION

The present work offers an extension of the well-known binary neuronal network model beyond the stationary case [9–11, 27]. We here describe the influence of a sinusoidally modulated input on the mean activities and the pairwise correlations to study the statistics of recurrently generated network activity in an oscillatory regime, ubiquitously observed in cortical activity [38].

Comparing with the results of the simulation of the binary network and the numerical solution of the full mean-field ODE, we are able to show that linear perturbation theory is enough to explain the most important effects occurring due to sinusoidal drive. This enables us to understand the system by the help of analytical expressions and furthermore we can predict its response to any time-dependent perturbation with existing Fourier representation by decomposing the perturbing input into its Fourier components.

We find that the amplitude of the modulation of the mean activity is of the order  $\frac{h_{\text{ext}}}{\sqrt{(1-\lambda_\alpha)^2 + (\tau\omega)^2}}$ , where  $\lambda_\alpha, \alpha \in \{E, I\}$  are the eigenvalues of the effective connectivity matrix  $W$ , i.e. the input is filtered by a first order low-pass filter with the amplitude of modulation decaying like  $\propto \omega^{-1}$  for large frequencies. This finding is in line with earlier work on the network susceptibility [9, esp. section V].

The qualitatively new result here is the identification of the mechanisms by which correlations  $\delta c$  are modulated in time. We find that on the one hand, correlations are driven by the direct modulation of the susceptibility  $S$  by the time-dependent external input, which leads to a term with a first order low-pass filter characteristic that dominates the modulated correlations at large frequencies. For small - and probably biologically realistic - frequencies (typically the LFP shows oscillations in the  $\beta$ -range around 20Hz), however, two other terms are equally important: First, the modulated mean activity leads to an additional modulation of the susceptibility. Second, time-modulated auto-correlations, analogous to the stationary setting [11], drive the pairwise correlations. Because the mean activity follows the external drive in a low-pass filtered manner, these two terms follow a second order low-pass-filter characteristics. These contributions are hence important at small frequencies, which are those we are interested in. The two terms modulating the susceptibility, by the direct input and the feedback of the mean activity through the network, have opposite signs in balanced networks. Together with their different frequency dependence, this leads to their summed absolute value having a maximum. In EI-networks, this can even be so if the effective connectivity  $W$  has only real eigenvalues and therefore the mean activity shows non-resonant behavior. However, whether the total dependence of  $\delta c$  on the perturbing frequency shows resonant behavior depends also on the third term coming from the modulated auto correlations. We find that in purely inhibitory networks, the resonance peak is typically overshadowed by the latter term. This is because inhibitory feedback leads to negative average pairwise correlations [11], which we show here reduce the driving force for the two resonant contributions. In balanced E-I networks, the driving force is less reduced by cancellation of correlations, so the resonant contribution can become dominant.

For the biologically motivated parameters used in the last setting the effective coupling matrix  $W$  has complex eigenvalues leading to a resonant mode at frequency  $f_{\text{res}}$  already in the mean activities. For an inhomogeneity independent of the driving frequency,  $\delta c$  has resonant modes with frequency  $f_{\text{res}}$  and  $2f_{\text{res}}$ . However, due to the mixing of the different modes and the fact that the inhomogeneity in the ODE for  $\delta c$  depends on  $\delta m$  and is therefore not constant, these resonances give only a hint on the “interesting” range for a perturbing frequency that would cause a maximal response. Especially the resonances are not sharp enough to be visible in any combination of the modes. Different behavior is expected near the critical point, i.e. near  $\Re(\lambda) \lesssim 1$ . For predictions of experimental results, however, a more careful choice of reasonable biological parameters would be necessary. In particular, the external drive should be gauged such that the modulations of the mean activities are in the experimentally observed range. Still, our setup shows that the theory presented here works in the biologically plausible parameter range.

A possible application of the framework developed in this paper is a quantitative comparison of the neuronal activity in the model network to the analysis of data measured in cortex [8]. Detecting the occurrence of so called unitary events (UE, [39, 40]), the authors observed that the simultaneous activation of neurons above the level expected for independence is locked to certain phases of the LFP. They hypothesized that the reason for this observation is the activation of cell assemblies. The results presented here show that the correlated activation of pairs of neurons is modulated by a sinusoidal drive even in a completely unstructured random network. In consequence, the locking of pairwise events to the cycle of the local field potential is more pronounced for correlated events than for single spikes. Future work needs to quantitatively compare experimental data to the results from the model presented here. The closed form expressions for the modulations of the mean activities and covariances enable such an approach and the effective study of the dependence on the model parameters. A quantitative comparison needs to convert mean activities and pairwise correlations for binary neurons into the probability to measure a unitary event, interpreting the binary neuron states as binned spike trains. Preliminary results indicate that already the homogeneous network

presented in this paper can show some features described in [8]. The presented methods will help to analyze the modulation of correlations in the presence of cell assemblies [41] in the model. This can easily be done by enhancing the connection probability among groups of excitatory neurons, similar as in [42] and will give a more realistic model that is able to capture also non-linear effects. Technically this extension amounts to the introduction of additional populations and the change of the connectivity matrix to reflect that these populations represent cell assemblies.

The relation of spiking activity to mesoscopic measures, such as the LFP, is still an open question. These population measures of neuronal activity naturally depend on the statistics of the microscopic activity they are composed of. Pairwise correlations, the focus of the current work, in particular tend to dominate the variance of any mesoscopic signal of summed activity: The contribution of cross-correlations grows quadratically in the number of components, autocorrelations only linearly [43, Box 2][14, eq. (1)][4, eq. (1),(2)]. Under the assumption that the LFP mainly reflects the input to a local recurrent network [4, 7], we have shown here that these two signals - spikes and LFPs - are intimately related; not only does the afferent oscillatory drive trivially modulate the propensity to produce spikes, i.e. the firing rate, but also the joint statistics of pairs of neurons by the three distinct mechanisms exposed in the present analysis. Forward modeling studies have shown that the spatial reach of the LFP critically depends on pairwise correlations, with elevated correlations leading to larger reach [4]. In this light our work shows that a local piece of neuronal tissue driven by a source of coherent oscillations will more effectively contribute to the local field potential itself: not only the spiking rate is modulated accordingly, but also the correlations are increased and decreased in a periodic manner, further amplifying the modulation of the generated local field potential and temporally modulating the spatial reach of the signal.

Functional consequences of the findings presented here deduce from the hypothesis that communication channels in cortex may effectively be multiplexed by the selective excitation of different areas with coherent oscillations [44, 45]. The presented analysis exposes that oscillatory drive to a local piece of cortex alone already effectively enhances coherent firing beyond the level expected based on the assumption of independence. If synchronous activity is employed as a dimension to represent information, it is hence tightly entangled with time-dependent changes of the mean activity. A similar conclusion was drawn from the observation that correlation transmission in feed-forward networks is monotonously increasing with firing rate [46, 47]. Any information-carrying modulation of synchronous activity must hence go beyond the here investigated effects, which can be regarded the baseline given by the non-stationary activity in networks without function. Since the mechanisms we have exposed only depend on generic features of cortical tissue - networks of non-linear neurons, connectivity with strong convergence and divergence, and dynamic stabilization by inhibition - the time-dependent entanglement of mean activity and correlations qualitatively exists in any network with these properties. In this view, our analysis can help to distinguish the level of time-modulated correlations in neural tissues that are surprising, and are therefore candidates to be attributed to function, from those that need to be expected in networks due to their generic properties.

## APPENDIX

### Derivation of theoretical results

#### *Derivation of the moment equations using the Master equation*

For completeness, we here derive the differential equations equations for the first and second moments (14), following previous work [9, 11, 13, 28, 29].

We multiply the Master equation by  $n_k$  or  $n_l n_k$  respectively and get



$$\begin{aligned}
\tau \frac{d}{dt} \langle n_k \rangle (t) &= \sum_{\mathbf{n} \in \{0,1\}^N} \frac{d}{dt} p(\mathbf{n}, t) n_k = \sum_{\mathbf{n} \setminus n_k} n_l \phi_k(\mathbf{n} \setminus n_k, t) \\
&= \sum_{\mathbf{n} \in \{0,1\}^N} n_k \sum (2n_i - 1) \phi_i(\mathbf{n} \setminus n_i, t) \\
&= \sum_{\mathbf{n} \in \{0,1\}^N} \left( n_k \phi(\mathbf{n} \setminus n_k, t) + \underbrace{n_k \sum_{i \neq k}^N (2n_i - 1) \phi_i(\mathbf{n} \setminus n_i, t)}_{=0} \right) \\
&= \sum_{\mathbf{n} \setminus n_k} [-p(\mathbf{n}_{k+}, t) + (p(\mathbf{n}_{k-}, t) F_k(\mathbf{n}_{k-}) + p(\mathbf{n}_{k+}, t) F_k(\mathbf{n}_{k+}))] \\
&= -\langle n_k \rangle (t) + \langle F_k(t) \rangle
\end{aligned}$$

and

$$\begin{aligned}
\frac{d}{dt} \langle n_k(t) n_l(t) \rangle &= \sum_{\mathbf{n} \in \{0,1\}^N} \frac{d}{dt} p(\mathbf{n}, t) n_k n_l \\
&= \sum_{\mathbf{n} \in \{0,1\}^N} n_k n_l \sum_{i=1}^N (2n_i - 1) \phi_i(\mathbf{n} \setminus n_i, t) \\
&= \sum_{\mathbf{n} \in \{0,1\}^N} (n_k n_l \phi_k(\mathbf{n} \setminus n_k, t) + n_l n_k \phi_l(\mathbf{n} \setminus n_l, t) \\
&\quad + \underbrace{n_k n_l \sum_{i \neq k, l}^N (2n_i - 1) \phi_i(\mathbf{n} \setminus n_i, t)}_{=0}) \\
&= \sum_{\mathbf{n} \setminus n_k} n_l \phi_k(\mathbf{n} \setminus n_k, t) + k \leftrightarrow l \\
&= \sum_{\mathbf{n} \setminus n_k} [-n_l p(\mathbf{n}_{k+}, t) + n_l (p(\mathbf{n}_{k-}, t) F_k(\mathbf{n}_{k-}) + p(\mathbf{n}_{k+}, t) F_k(\mathbf{n}_{k+}))] \\
&\quad + k \leftrightarrow l \\
&= \{-\langle n_k(t) n_l(t) \rangle + \langle n_l(t) F_k(t) \rangle\} + \{k \leftrightarrow l\}.
\end{aligned}$$

*Two signals with correlation coefficient varying in time described by an Ornstein-Uhlenbeck process*

As a minimal example including time-dependent zero-time lag correlations, we produce two stochastic processes whose correlation changes with time. To be more precise, there are three independent realizations of Ornstein-Uhlenbeck processes (OUP)  $s_i(t)$ ,  $i \in \{1, 2, c\}$ , all obeying the ODE  $\tau \frac{d}{dt} s_i(t) = -s_i(t) + \xi_i(t)$ , where  $\xi$  is a stochastic variable fulfilling  $\langle \xi_i(t) \rangle = 0$ ,  $\langle \xi_i(t)^2 \rangle = \tau \sigma^2 \delta(t)$ . This leads to ( $t_0$  is the initial time point, could be set to 0)

$$\langle (s_i(t) - \langle s_i(t) \rangle)^2 \rangle = \frac{\sigma^2}{2} \left( 1 - e^{-2 \frac{t-t_0}{\tau}} \right).$$

After evaluating the OUP numerically, we take only the solution after the transient time, so that  $\langle (s_i(t) - \langle s_i(t) \rangle)^2 \rangle \approx \frac{\sigma^2}{2} \forall i$  constantly and define the stochastic processes  $x_i$ ,  $i \in \{1, 2\}$  to be

$$\begin{aligned}
x_1(t) &= \sin(\omega t) + \sqrt{c(t)} s_c(t) + \sqrt{1-c(t)} s_1(t) \\
x_2(t) &= \cos(\omega t) + \sqrt{c(t)} s_c(t) + \sqrt{1-c(t)} s_2(t), \\
\text{where } c(t) &= \frac{1}{1 + \exp((t - \frac{T}{2})/d)}.
\end{aligned}$$

Note that  $s_i(t)$ ,  $i \in \{1, 2, c\}$  are only auxiliary variables, especially their time-dependence is neglected and is even rather undesirable. Ideally, the whole time-dependence would be included in  $c(t)$ . We also could have chosen unfiltered Gaussian variables for every time step, but used the filtering through the OUP to ameliorate the readability of the plots in Figure 2. There is yet another motivation to introduce OUP here: The time-dependence of the first two moments of the networks considered in this work can be described by a (driven) OUP to first order, so the qualitative picture could even be made more quantitative [23].

### Extracting the correct phase from complex solutions

Notice that there are a few subtleties to keep in mind when a discrete Fourier transform is applied to  $\delta m_\alpha$ . The (in both senses) real-valued solution of the ODE is

$$\begin{aligned}\delta m_\alpha &= \Im(M_\alpha^1 e^{i\omega_0 t}) = \Im(|M_\alpha^1| e^{i(\arg(M_\alpha^1) + \omega_0 t)}) = |M_\alpha^1| \sin(\arg(M_\alpha^1) + \omega_0 t) \\ &= |M_\alpha^1| (\sin(\arg(M_\alpha^1)) \cos(\omega_0 t) + \cos(\arg(M_\alpha^1)) \sin(\omega_0 t)).\end{aligned}$$

For clarity, we here named the driving frequency  $\omega_0$ . Therefore, if we calculate the Fourier transform (in a distributional sense), we get

$$\begin{aligned}\mathcal{F}[\delta m_\alpha](\omega = \omega_0) &= |M_\alpha^1| \left( \sin(\arg(M_\alpha^1)) \frac{\delta_{\omega_0} + \delta_{-\omega_0}}{2} + \cos(\arg(M_\alpha^1)) \frac{\delta_{\omega_0} - \delta_{-\omega_0}}{2i} \right) \\ &= \frac{|M_\alpha^1|}{2} (\delta_{\omega_0} (\sin(\arg(M_\alpha^1)) - i \cos(\arg(M_\alpha^1))) + \delta_{-\omega_0} (\sin(\arg(M_\alpha^1)) + i \cos(\arg(M_\alpha^1))))\end{aligned}$$

Thus, we get

$$|\mathcal{F}[\delta m_\alpha](\omega_0)| = |\mathcal{F}[\delta m_\alpha](-\omega_0)| = \frac{|M_\alpha^1|}{2}$$

and, because we take the imaginary part of the complex solution which leads to a  $\frac{\pi}{2}$ -phase shift compared to the complex phase

$$\Leftrightarrow \arg(\mathcal{F}[\delta m_\alpha](\omega_0)) = \begin{cases} \arg(M_\alpha^1) + \frac{3\pi}{2}, & \text{for } \arg(M_\alpha^1) \in [-\pi, -\frac{\pi}{2}] \\ \arg(M_\alpha^1) - \frac{\pi}{2}, & \text{for } \arg(M_\alpha^1) \in (-\frac{\pi}{2}, \pi) \end{cases}.$$

### Comparison of simulation and theory of the ei and ii-correlations

For completeness, we include here the plots showing the dependence of the correlations between inhibitory and inhibitory and excitatory on the driving frequency for the third network setup of the main text.

### Acknowledgments

The authors would like to thank PierGianLuca Porta Mana for his great support and Michael Denker, Sonja Grün and the whole INM-6 for fruitful discussions. This work was partly supported by the Helmholtz young investigator group VH-NG-1028, the Helmholtz Portfolio Supercomputing and Modeling for the Human Brain (SMHB) and EU Grant 604102 (Human Brain Project, HBP). All network simulations carried out with NEST (<http://www.nest-simulator.org>).

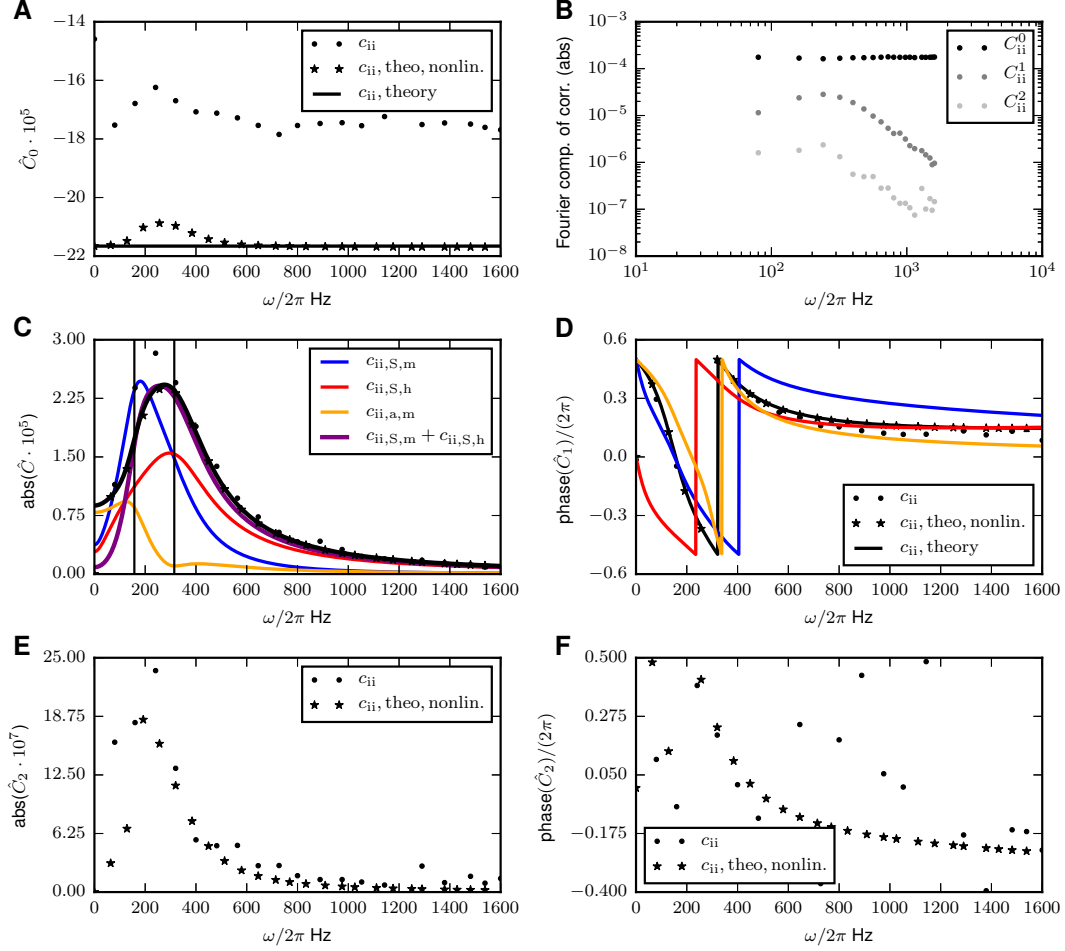


Figure 9. **Driven E-I network with biologically inspired parameters: II-Covariance.** Response of the inh.-inh.-part of the covariance to a perturbation with frequency  $\omega$  in the Fourier space. The first row (A) shows the zeroth order, i.e. the constant part, the second (C,D) and third rows (E,F) show the absolute value and the complex phase of the first and second Fourier coefficients. A Zeroth order (time independent part) of the covariance. B Absolute value of the first three Fourier components of the  $c_{ii}$ -correlations in loglog-scale. C Absolute value of the first order of the time-dependent part of the covariance. D Phase angle in relation to the driving signal. E and F are structured analogous to C and D for the second Fourier modes. Solid lines indicate the linear theory (31), stars the results of the numerical solved full mean-field theory (5) and (6) and dots those of the direct simulation of the full network. Numerical results obtained by the same methods and with the same parameters as in Figure 3.

- 
- [1] Scherberger H, Jarvis MR, Andersen RA. Cortical Local Field Potential Encodes Movement Intentions in the Posterior Parietal Cortex. *Neuron*. 2005;46(2):347 – 354. Available from: <http://www.sciencedirect.com/science/article/pii/S0896627305001996>.
  - [2] Nunez PL, Ramesh S. Electric fields of the brain: the neurophysics of EEG. Oxford University Press; 2006.
  - [3] Ray S, Crone NE, Niebur E, Franaszczuk PJ, Hsiao SS. Neural correlates of high-gamma oscillations (60-200 Hz) in macaque local field potentials and their potential implications in electrocorticography. *J Neurosci*. 2008 November;28(45):11526–11536.
  - [4] Lindén H, Tetzlaff T, Potjans TC, Pettersen KH, Grün S, Diesmann M, et al. Modeling the spatial reach of the LFP. *Neuron*. 2011;72(5):859–872.
  - [5] Mitzdorf U. Current Source-Density Method and Application in Cat Cerebral Cortex: Investigation of Evoked Potentials and EEG Phenomena. *Physiol Rev*. 1985;65(1):37–100.
  - [6] Viswanathan A, Freeman RD. Neurometabolic coupling in cerebral cortex reflects synaptic more than spiking activity. *Nature Neuroscience*. 2007;10:1308 – 1312.

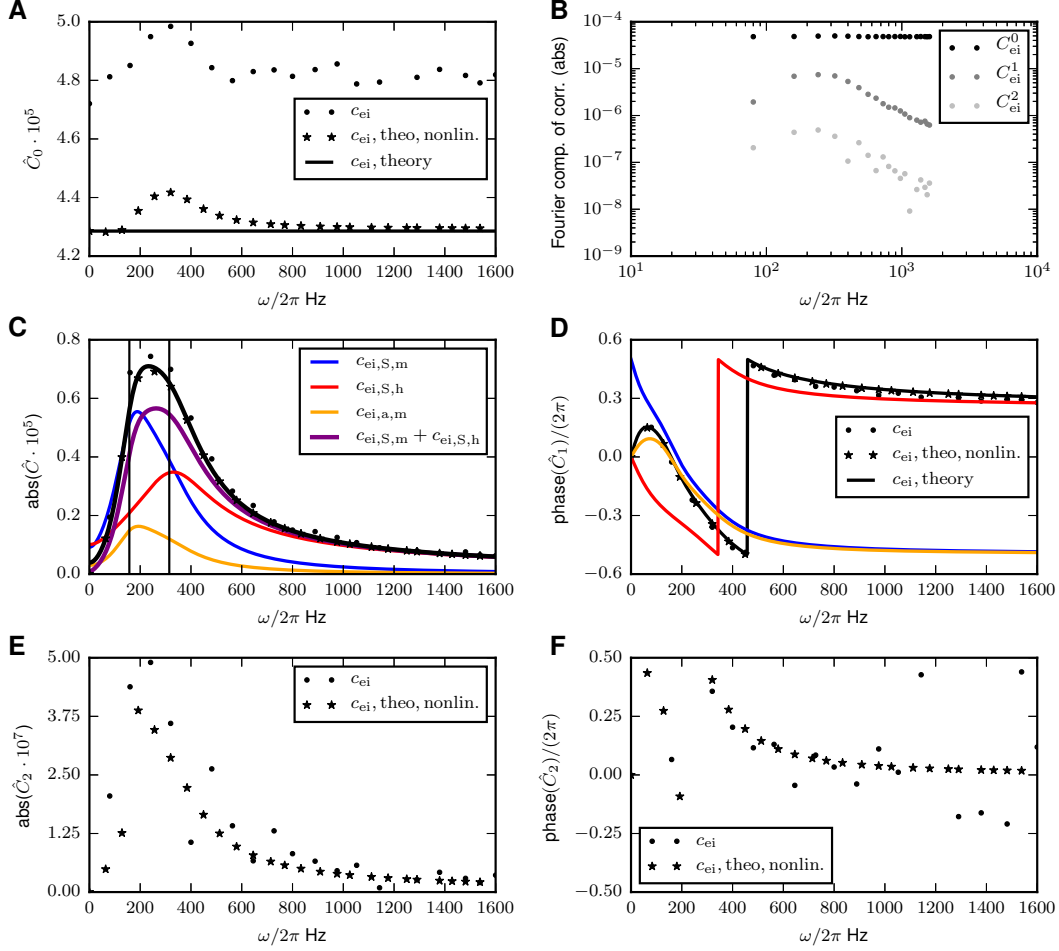


Figure 10. **Driven E-I network with biologically inspired parameters: EI-Covariance.** Response of the exc.-inh.-part of the covariance to a perturbation with frequency  $\omega$  in the Fourier space. The first row (A) shows the zeroth order, i.e. the constant part, the second (C,D) and third rows (E,F) show the absolute value and the complex phase of the first and second Fourier coefficients. **A** Zeroth order (time independent part) of the covariance. **B** Absolute value of the first three Fourier components of the  $c_{ei}$ -correlations in loglog-scale. **C** Absolute value of the first order of the time-dependent part of the covariance. **D** Phase angle in relation to the driving signal. **E** and **F** are structured analogous to **C** and **D** for the second Fourier modes. Solid lines indicate the linear theory (31), stars the results of the numerical solved full mean-field theory (5) and (6) and dots those of the direct simulation of the full network. Numerical results obtained by the same methods and with the same parameters as in Figure 3.

- [7] Mazzoni A, Lindén H, Cuntz H, Lansner A, Panzeri S, Einevoll G. Computing the Local Field Potential (LFP) from Integrate-and-Fire Network Models. *PLoS Comput Biol.* 2015;11:1–38.
- [8] Denker M, Roux S, Lindén H, Diesmann M, Riehle A, Grün S. The Local Field Potential Reflects Surplus Spike Synchrony. *Cereb Cortex.* 2011 December;21:2681–2695.
- [9] Ginzburg I, Sompolinsky H. Theory of correlations in stochastic neural networks. *Phys Rev E.* 1994;50(4):3171–3191.
- [10] Van Vreeswijk C, Sompolinsky H. Chaotic balanced state in a model of cortical circuits. *Neural Comput.* 1998;10(6):1321–1371.
- [11] Helias M, Tetzlaff T, Diesmann M. The correlation structure of local cortical networks intrinsically results from recurrent dynamics. *PLoS Comput Biol.* 2014;10(1):e1003428.
- [12] van Vreeswijk C, Sompolinsky H. Chaos in Neuronal Networks with Balanced Excitatory and Inhibitory Activity. *Science.* 1996 December, 6;274:1724–1726.
- [13] Renart A, De La Rocha J, Bartho P, Hollender L, Parga N, Reyes A, et al. The asynchronous State in Cortical Circuits. *Science.* 2010 January;327:587–590.
- [14] Tetzlaff T, Helias M, Einevoll G, Diesmann M. Decorrelation of neural-network activity by inhibitory feedback. *PLoS Comput Biol.* 2012;8(8):e1002596.

- [15] Oppenheim A, Wilsky A. Systems and signals. Prentice Hall; 1996.
- [16] Amit DJ, Brunel N. Dynamics of a recurrent network of spiking neurons before and following learning. *Network: Comput Neural Systems*. 1997;8:373–404.
- [17] Shadlen MN, Newsome WT. Noise, neural codes and cortical organization. *Curr Opin Neurobiol*. 1994;4(4):569–579.
- [18] Softky WR, Koch C. The Highly Irregular Firing of Cortical Cells Is Inconsistent with Temporal Integration of Random EPSPs. *J Neurosci*. 1993;13(1):334–350.
- [19] Brunel N, Hakim V. Fast Global Oscillations in Networks of Integrate-and-Fire Neurons with Low Firing Rates. *Neural Comput*. 1999;11(7):1621–1671.
- [20] Lindner B, Schimansky-Geier L. Transmission of noise coded versus additive signals through a neuronal ensemble. *Phys Rev Lett*. 2001;86:2934–2937.
- [21] Richardson MJE. Spike-train spectra and network response functions for non-linear integrate-and-fire neurons. *Biol Cybern*. 2008;99:381–392.
- [22] Brunel N, Latham P. Firing rate of the noisy quadratic integrate-and-fire neuron. *Neural Comput*. 2003;15(10):2281–2306.
- [23] Grytskyy D, Tetzlaff T, Diesmann M, Helias M. A unified view on weakly correlated recurrent networks. *Front Comput Neurosci*. 2013;7:131.
- [24] Gewaltig MO, Diesmann M. NEST (NEural Simulation Tool). *Scholarpedia*. 2007;2(4):1430.
- [25] Eppler JM, Pauli R, Peyser A, Ippen T, Morrison A, Senk J, et al.. NEST 2.8.0; 2015. Available from: <http://dx.doi.org/10.5281/zenodo.32969>.
- [26] van Vreeswijk C, Sompolinsky H. Chaotic Balanced State in a Model of Cortical Circuits. *Neural Comput*. 1998;10:1321–1371.
- [27] Buice MA, Cowan JD, Chow CC. Systematic fluctuation expansion for neural network activity equations. *Neural Comput*. 2010 Feb;22(2):377–426. Available from: <http://www.ncbi.nlm.nih.gov/pmc/articles/PMC2805768/>.
- [28] Glauber R. Time-dependent statistics of the Ising model. *J Math Phys*. 1963;4(2):294–307.
- [29] Buice MA, Cowan JD, Chow CC. Systematic Fluctuation Expansion for Neural Network Activity Equations. *Neural Comput*. 2009;22:377–426.
- [30] van Vreeswijk C. What Is the Neural Code? In: van Hemmen L, Sejnowski T, editors. *23 Problems in Systems Neuroscience*. Oxford University Press; 2006. p. 143–159.
- [31] Dahmen D, Bos H, Helias M. Correlated fluctuations in strongly-coupled binary networks beyond equilibrium. *arXiv*. 2015;1512.01073 [q-bio.NC]. Available from: <http://arxiv.org/abs/1512.01073>.
- [32] Jones E, Oliphant T, Peterson P, et al.. SciPy: Open source scientific tools for Python; 2001. [Http://www.scipy.org/](http://www.scipy.org/).
- [33] Yoshimura Y, Callaway EM. Fine-scale specificity of cortical networks depends on inhibitory cell type and connectivity. *Nat Neurosci*. 2005;8(11):1552–1559.
- [34] Avermann M, Tömm C, Mateo C, Gerstner W, Petersen C. Microcircuits of excitatory and inhibitory neurons in layer 2/3 of mouse barrel cortex. *J Neurophysiol*. 2012;107(11):3116–3134.
- [35] Lefort S, Tömm C, Sarria JCF, Petersen CCH. The Excitatory Neuronal Network of the C2 Barrel Column in Mouse Primary Somatosensory Cortex. *Neuron*. 2009;61(2):301–316. Available from: <http://www.sciencedirect.com/science/article/pii/S0896627308010921>.
- [36] Gentet L, Avermann M, Matyas F, Staiger JF, Petersen CCH. Membrane Potential Dynamics of GABAergic Neurons in the Barrel Cortex of Behaving Mice. *Neuron*. 2010;65:422–435.
- [37] Cichocki A, Zdunek R, Phan AH, Amari Si. Nonnegative matrix and tensor factorizations: applications to exploratory multi-way data analysis and blind source separation. John Wiley & Sons; 2009.
- [38] Buzsáki G, Draguhn A. Neuronal Oscillations in Cortical Networks. *Science*. 2004;304:1926–1929.
- [39] Grün S, Diesmann M, Aertsen A. ‘Unitary Events’ in Multiple Single-Neuron Spiking Activity. I. Detection and Significance. *Neural Comput*. 2002;14(1):43–80.
- [40] Grün S, Diesmann M, Aertsen A. ‘Unitary Events’ in Multiple Single-Neuron Spiking Activity. II. Non-Stationary Data. *Neural Comput*. 2002;14(1):81–119.
- [41] Yoshimura Y, Dantzker JLM, Callaway EM. Excitatory cortical neurons form fine-scale functional networks. *Nature*. 2005;433(24):868–873.
- [42] Litwin-Kumar A, Chacron MJ, Doiron B. The Spatial Structure of Stimuli Shapes the Timescale of Correlations in Population Spiking Activity. *PLoS Comput Biol*. 2012;8(9):e1002667.
- [43] Harris KD, Thiele A. Cortical state and attention. *Nat Rev Neurosci*. 2011 September;12:509–523.
- [44] Singer W. Neuronal synchrony: a versatile code for the definition of relations? *Neuron*. 1999 Sep;24(1):49–65.
- [45] Womelsdorf T, Schoffelen JM, Oostenveld R, Singer W, Desimone R, Engel AK, et al. Modulation of Neuronal Interactions Through Neuronal Synchronization. *Science*. 2007 June;316(15):1609–1612.
- [46] De la Rocha J, Doiron B, Shea-Brown E, Kresimir J, Reyes A. Correlation between neural spike trains increases with firing rate. *Nature*. 2007 august;448(16):802–807.
- [47] Shea-Brown E, Josic K, de la Rocha J, Doiron B. Correlation and synchrony transfer in integrate-and-fire neurons: basic properties and consequences for coding. *Phys Rev Lett*. 2008 March;100:108102.